

2016-12-09

Controls on the early Holocene collapse of the Bothnian Sea Ice Stream

Clason, Caroline

<http://hdl.handle.net/10026.1/8106>

10.1002/2016JF004050

Journal of Geophysical Research: Earth Surface

American Geophysical Union (AGU)

All content in PEARL is protected by copyright law. Author manuscripts are made available in accordance with publisher policies. Please cite only the published version using the details provided on the item record or document. In the absence of an open licence (e.g. Creative Commons), permissions for further reuse of content should be sought from the publisher or author.

1 **Controls on the early Holocene collapse of the Bothnian Sea Ice Stream**

2
3 **Caroline C. Clason^{1,2*}, Sarah L. Greenwood³, Nick Selmes⁴, James M. Lea^{5,2,6}, Stewart**
4 **S.R. Jamieson⁷, Faezeh M. Nick⁸ and Per Holmlund²**

5 ¹School of Geography, Earth and Environmental Sciences, Plymouth University, Plymouth,
6 PL4 8AA, UK

7 ²Department of Physical Geography, Stockholm University, 106 91 Stockholm, Sweden

8 ³Department of Geological Sciences, Stockholm University, 106 91 Stockholm, Sweden

9 ⁴Plymouth Marine Laboratory, Plymouth, PL1 3DH, UK

10 ⁵Geography and Planning, University of Liverpool, Liverpool, L69 7ZT, UK

11 ⁶Bolin Centre for Climate Research, Stockholm University, 106 91 Stockholm, Sweden

12 ⁷Department of Geography, Durham University, Durham, DH1 3LE, UK

13 ⁸University Centre in Svalbard (UNIS), P.O. Box 156, Longyearbyen, Norway

14
15 *Corresponding author: Caroline Clason (caroline.clason@plymouth.ac.uk)
16

17 **Key Points:**

- 18 • We apply a flowline model to test sensitivity of the Bothnian Sea Ice Stream to
19 external forcings.
- 20 • Model experiments, supported by geomorphological analyses, suggest that ice stream
21 retreat was meltwater-driven.
- 22 • Despite the marine setting, it is likely that the ice stream was relatively insensitive to
23 marine forcings.
24
25

26

27

28

29

30

31

32

33

34

35 Abstract

36

37 New high resolution multibeam data in the Gulf of Bothnia reveal for the first time the
38 subglacial environment of a Bothnian Sea Ice Stream. The geomorphological record suggests
39 that increased meltwater production may have been important in driving rapid retreat of
40 Bothnian Sea ice during deglaciation. Here we apply a well-established one-dimensional
41 flowline model to simulate ice flow through the Gulf of Bothnia and investigate controls on
42 retreat of the ice stream during the post-Younger Dryas deglaciation of the Fennoscandian Ice
43 Sheet. The relative influence of atmospheric and marine forcings are investigated, with the
44 modelled ice stream exhibiting much greater sensitivity to surface melting, implemented
45 through surface mass balance and hydrofracture-induced calving, than to submarine melting
46 or relative sea level change. Such sensitivity is supported by the presence of extensive
47 meltwater features in the geomorphological record. The modelled ice stream does not
48 demonstrate significant sensitivity to changes in prescribed ice stream width or overall bed
49 slope, but local variations in basal topography and ice stream width result in non-linear retreat
50 of the grounding line, notably demonstrating points of short-lived retreat slowdown on reverse
51 bed slopes. Retreat of the ice stream was most likely governed by increased ice surface
52 meltwater production, with the modelled retreat rate less sensitive to marine forcings despite
53 the marine setting.

54

55

56 1. Introduction

57

58 Marine-terminating glaciers are a major source of mass loss from the contemporary
59 Greenland and Antarctic ice sheets (Van den Broeke et al., 2009; Cook et al., 2014; Murray et
60 al., 2015), sensitive to both atmospheric and marine forcings, and thus particularly susceptible
61 to climatic and environmental changes. Submarine melting is often considered one of the
62 most important drivers of marine-terminating glacier retreat due to the potential to drive ice
63 shelf de-buttressing and consequent dynamic thinning (Joughin and Alley, 2011; Luckman et
64 al., 2015). Where the bed increases in depth upstream this can lead to a runaway effect
65 referred to as marine ice sheet instability (Weertman, 1974; Schoof, 2007), with an increase in
66 grounding line depth leading to increased ice flux due to thicker ice and increased calving.
67 Changes in both sea level and tides can influence the depth of the grounding line, with tides
68 further acting to modulate ice velocities and hydrostatic backstress (Anandakrishnan et al.,
69 2003; Thomas, 2007). Local topography can also control grounding line retreat, with reverse
70 bed slopes increasing the risk of instability, while topographic highs can create pinning points
71 for stabilisation. In addition, the sides of troughs can exert a lateral drag, reducing ice flow
72 and slowing retreat (Whillans and van der Veen, 1997), with some evidence for a narrowing
73 in ice stream width aiding short-lived slowdown of retreat on reverse bed slopes
74 (Gudmundsson et al., 2012; Jamieson et al., 2012).

75

76 In addition to marine forcings, the stability of marine-terminating glaciers can also be strongly
77 influenced by atmospheric warming (Lea et al., 2014a; DeConto and Pollard, 2016). Changes
78 in accumulation and ablation can induce thinning promoting a dynamic response, while
79 meltwater reaching the ice-bed interface can enhance basal lubrication and alter the efficiency
80 and topology of the subglacial hydrological system, further perturbing ice dynamics in at least
81 the sub-annual scale (Zwally et al., 2002; Sole et al., 2013; Doyle et al., 2014). Surface
82 meltwater can also induce hydrofracture of crevasses leading to increased rates of calving
83 (Benn et al., 2007; Colgan et al., 2016), and can indirectly cause increased submarine melting

84 through the release of supraglacially-originating plumes of subglacial meltwater at glacier
85 termini (Motyka et al., 2003; Chauché et al., 2014). The relative contribution of these
86 individual external forcings on the dynamics and stability of marine-terminating glaciers
87 remains poorly constrained (Nick et al., 2009, 2010, 2012; Murray et al., 2010; Straneo et al.,
88 2013), providing major uncertainty in understanding their stability and retreat, compounded
89 by the interlinked nature of, and non-linear feedbacks between forcings. To better predict
90 future response of these catchments, it is imperative to better understand the physical
91 processes and local factors determining grounding line stability and retreat behaviour in a
92 diverse range of settings.

93
94 The record of well-constrained observations of contemporary marine-terminating catchments
95 is short (Kjeldsen et al., 2015; Murray et al., 2015), and only informs us of ice flow behaviour
96 on the order of hours to decades (Joughin et al., 2010). However, the geological record of
97 these catchments' dynamics can improve our understanding of the roles of climate, marine
98 processes and topography on marine ice stream retreat, particularly over centennial to
99 millennial timescales (Winsborrow et al., 2010; Jakobsson et al., 2011; Jamieson et al., 2014;
100 Jones et al., 2015). In particular, landform assemblages created by past ice flow regimes and
101 grounding line processes provide important constraints on physical models of glaciological
102 processes. This work presents a combined geomorphological and modelling approach to
103 examining the controls on the retreat and dynamics of a palaeo ice stream in the Gulf of
104 Bothnia. We investigate this setting because (i) the epicontinental, c. 100,000 km² basin
105 contrasts with the ocean-facing, continental shelf trough environments that have hitherto been
106 the focus of marine ice instability investigation; (ii) the retreat pattern, controls and effect of
107 this major ice flow corridor on southern Fennoscandian Ice Sheet (FIS) deglaciation are
108 currently poorly understood; and (iii) the availability of excellent new geomorphological data
109 constrain its behaviour.

110
111 Here we apply a well-established numerical flowline model (Vielé and Payne, 2005; Nick et
112 al., 2010) to investigate the relative sensitivity of Bothnian Sea ice stream retreat to both
113 atmospheric and marine forcings. Specifically, we examine the effects of increased ice surface
114 melting, submarine melting at the terminus, and sea level change, in addition to sensitivity to
115 basal topography and catchment geometry. A newly reported, rich landform record of
116 deglaciation (Greenwood et al., in press), coupled with a physical exploration of ice sheet
117 retreat processes, provide an opportunity to gain an improved understanding of the balance of
118 processes governing a major marine ice sheet catchment, and ultimately its stability.

119
120

121 **2. The Geomorphological Record of Palaeo-Ice Flow**

122

123 The Gulf of Bothnia is a shallow, epicontinental basin that lies in the heart of the terrain
124 formerly covered by the FIS (figure 1). The Bothnian Bay sub-basin, in the north, is separated
125 from the larger Bothnian Sea to the south by a shallow sill; the Bothnian Sea is similarly
126 separated from the Baltic Sea by the Åland archipelago. These basins are thought to have
127 hosted a variety of glaciodynamic environments throughout the evolution of the FIS: an
128 interior position close to the main ice divide (Kleman et al., 1997), the head of an extensive
129 Baltic Ice Stream (Holmlund and Fastook, 1993; Boulton et al., 2001), and a major corridor of
130 marine- and lacustrine-based deglaciation (De Geer, 1940; Strömberg, 1989; Lundqvist,
131 2007). From the Younger Dryas and subsequent deglaciation, a series of ice lobes are
132 conventionally considered to have crossed the Gulf of Bothnia south-eastwards into Finland,
133 well-defined by glacial lineations, interlobate esker corridors, and large, lobate terminal

134 moraines (Punkari, 1980; Johansson et al., 2011). This whole sector deglaciated under marine
135 (periodically lacustrine) conditions (Björck, 1995; Andrén et al., 2011). The marine limit on
136 the Swedish High Coast is 286 m above present-day sea level (Berglund, 2004).

137
138 All reconstructions of palaeo-ice dynamics in the Bothnian basin have hitherto been drawn
139 from evidence from the present-day terrestrial domain; direct glacial geological or
140 geomorphological evidence from the Gulf itself has been almost entirely lacking, and the
141 dynamics of ice retreat are thus poorly understood. New, extensive, high-resolution
142 multibeam echo-sounding data allow direct investigation of its glacial geomorphological
143 record for the first time, revealing a palaeo-ice stream directed SSW-S-ward through the
144 Bothnian Sea (Greenwood et al., 2015; Greenwood et al., in press). Mega-scale glacial
145 lineations (MSGs) >20 km in length define a slightly sinuous, ~350 km long ice stream
146 pathway, with an onset zone over the Västerbotten coast of Sweden marked by distinct
147 transitions in lineation size and elongation (Greenwood et al., 2015). The width of this onset
148 zone is limited to ~40 km, while the ice stream trunk, indicated by increasing downstream
149 MSG length and elongation, continues to a position in the central-southern Bothnian Sea.
150 Here, MSGs overprint each other in 2-3 sub-parallel sets that together indicate a splayed,
151 lobate terminus. Beyond this position, small (55-700 m long) crag and tails and streamlined
152 crystalline bedrock exhibit convergent flow into the Åland Sea. We interpret initial retreat of
153 moderate-to-slow flowing ice across the Åland sill. A late-stage streaming event occurred as
154 ice retreated through the Gulf of Bothnia, but which did not extend the full length of the basin
155 and likely did not fill its entire breadth (Greenwood et al., in press).

156
157 Terrestrial-based chronologies for deglaciation provide an available time-window for
158 complete deglaciation of the Gulf of only c.1000-1200 years (Hughes et al., 2016; Stroeven et
159 al., 2016). This marks a 2- to 4-fold increase in the ice sheet retreat rate relative to the
160 deglaciation up until the Younger Dryas. Following retreat from the Younger Dryas position,
161 a notable lack of grounding line deposits suggests that there were no major standstills during
162 deglaciation (Greenwood et al., in press). The lobate and internally cross-cutting arrangement
163 of distal MSGs suggests the margin briefly paused at the terminus of the Bothnian Sea Ice
164 Stream, where the flow direction close to the grounding line shifted back and forth.
165 Approximately 160 km up-ice, a small group of transverse wedges suggest localised
166 grounding line pauses; otherwise, De Geer moraines only appear in the present-day coastal
167 and terrestrial domains, following loss of ice from the offshore sector. An extensive meltwater
168 landform record comprising interconnected channels, eskers and large (kilometre-scale)
169 erosional corridors suggest that meltwater access to and drainage via the subglacial system
170 was plentiful during deglaciation. These geomorphological observations indicate that retreat
171 of the Bothnian Sea ice sheet catchment was associated with episodically high ice flow
172 velocities, rapid margin retreat, high surface melting and access of supraglacial meltwater to
173 the bed.

174
175 Previous modelling of the FIS has largely focused on reproducing areal ice extent, and to a
176 lesser extent ice dynamics, at the ice sheet scale (Arnold and Sharp, 2002; Forsström et al.,
177 2003; Siegert and Dowdeswell, 2004; Clason et al., 2014). A number of modelling attempts
178 have reported difficulty in avoiding overly-rapid deglaciation through the Baltic-Bothnia
179 sector of the FIS (Holmlund and Fastook, 1993; Clason et al., 2014), with Holmlund and
180 Fastook (1993) resorting to the prescription of a “sticky spot” of cold-based ice over the
181 island of Åland (Figure 1) to decelerate ice sheet thinning and dam ice flow. Here we apply a
182 flowline model specifically to the Bothnian Sea case, to investigate the possible controls on
183 the retreat behaviour indicated by geomorphological evidence. We define an 835 km-long

184 central flowline in accordance with the MSGL assemblage and the small-scale lineations
 185 converging on the Sea of Åland. We specify a late-Younger Dryas terminal position (11.6 ka
 186 BP, based on the reconstructed margins of Stroeven et al. (2016), and extend our flowline
 187 headwards to the approximate position of a late-Younger Dryas ice divide (Kleman et al.,
 188 1997). We define a minimum width based on landform evidence of the palaeo-ice stream
 189 lateral margin, and allow a plausible maximum width to account for broader, non-streaming
 190 episodes and uncertainties due to restricted data coverage.

191
 192 Within this model set up, the defined flowline path is fixed for the duration of each model
 193 simulation. We consider the geometry of the modelled ice stream reasonable for the period of
 194 time in which ice is in the present-day offshore and nearshore domain. However, it is well-
 195 known that the FIS ice divide migrated west during this time and that the retreating flowline
 196 would also have swung westwards (Hughes et al., 2016; Stroeven et al., 2016). The uppermost
 197 part of our flowline should therefore be treated only as an accumulation zone for the distal,
 198 offshore ice dynamics, and not as an ultimately terrestrial retreat flowline.

199
 200

201 3. Numerical Modelling

202

203 3.1 Model description

204

205 We apply a well-established one-dimensional flowline model (Vieli and Payne, 2005),
 206 described in full in Nick et al (2010), to the Bothnian Sea case. The model has previously
 207 been applied to Greenland outlet glaciers in both contemporary (Nick et al., 2012; Carr et al.,
 208 2015) and historical (Lea et al., 2014a,b) settings, and used for the simulation of a palaeo ice
 209 stream in Antarctica by Jamieson et al. (2012; 2014). The model applies a non-linear effective
 210 pressure sliding law, with driving stress (left-hand term) balanced by the longitudinal stress
 211 gradient (first term), basal drag (second term) and lateral drag (third term) following van der
 212 Veen and Whillans (1996) and Fowler (2010), as

213

$$214 \quad \rho_i g H \frac{\partial h}{\partial x} = 2 \frac{\partial}{\partial x} \left(H v \frac{\partial U}{\partial x} \right) - \mu A_s \left[\left(H - \frac{\rho_p}{\rho_i} D \right) U \right]^{1/m} - \frac{2H}{W} \left(\frac{5U}{AW} \right)^{1/m} \quad (1)$$

215

216 where x is the distance along the flowline, h is the ice surface elevation, ρ_i is the density of
 217 ice, and ρ_p is proglacial water density which is held constant at 1000 kg m⁻³ to reflect the
 218 largely fresh or brackish water of the Late Weichselian Gulf of Bothnia (Björck, 1995;
 219 Andrén et al., 2000). g is acceleration due to gravity, U is the vertically-averaged horizontal
 220 ice velocity, H is the ice thickness, D is the depth of the base of the ice below the surface of
 221 the proglacial water body, A_s is the basal roughness parameter, W is glacier width, A is the
 222 temperature-dependent rate factor (Glen, 1955), μ is the basal friction parameter (typically 1,
 223 but can be modified to simulate meltwater-enhanced basal sliding), m is the friction exponent,
 224 and v is the strain rate-dependent effective viscosity, defined as

$$225 \quad v = A^{-\frac{1}{n}} \left| \frac{\partial U}{\partial x} \right|^{\frac{1-n}{n}} \quad (2)$$

226

227 where n is the exponent in Glen's flow law. Evolution of the ice thickness along the flowline
 228 accounts for changes in glacier width and surface mass balance, a , following

229

$$230 \quad \frac{\partial H}{\partial t} = \frac{1}{W} \frac{\partial q}{\partial x} + a \quad (3)$$

231 where q is the horizontal flux of ice through a cross-section of the flowline following $q =$
 232 HWU . Surface mass balance is implemented through a linear gradient which changes with
 233 elevation from a minimum at sea level to a maximum at the ice divide, with additional bounds
 234 set to restrict overly positive or negative values. The velocity boundary condition at the
 235 calving front is calculated as
 236

$$237 \frac{\partial U}{\partial x} = A \left[\frac{\rho_i g}{4} \left(H - \frac{\rho_p D^2}{\rho_i H} \right) \right]^n. \quad (4)$$

239 This condition balances the difference between the hydrostatic pressure of the ice and
 240 proglacial water with the stretching rate at the terminus. The model includes a physically-
 241 based full-depth calving criterion (Nick et al., 2010), which combines the depths of surface
 242 and basal crevasses within a field of closely-spaced crevasses (Nye, 1957; Benn et al., 2007).
 243 Surface crevasse depth, d_s , is determined by the longitudinal stresses and crevasse water
 244 level, following Benn et al. (2007), such that
 245

$$246 d_s = \frac{R_{xx}}{\rho_i g} + \frac{\rho_w}{\rho_i} d_w \quad (5)$$

248 where ρ_w is the density of meltwater, d_w is the depth of water in the crevasse, and R_{xx} is the
 249 normal resistive stress which relates to the longitudinal stretching rate, $\dot{\epsilon}_{xx}$, following Glen's
 250 flow law (van der Veen, 1999)
 251

$$252 R_{xx} = 2 \left(\frac{\dot{\epsilon}_{xx}}{A} \right)^{\frac{1}{n}}. \quad (6)$$

253 Tuning the water depth in surface crevasses thus allows for exploration of the effect of
 254 increased meltwater production on calving rates and grounding line retreat. The height of
 255 basal crevasses, d_b , is calculated following
 256

$$257 d_b = \frac{\rho_i}{\rho_p - \rho_i} \left(\frac{R_{xx}}{\rho_i g} - H_{ab} \right) \quad (7)$$

260 where H_{ab} is the height above buoyancy, following
 261

$$262 H_{ab} = H - \frac{\rho_p}{\rho_i} D. \quad (8)$$

264 The formation of a floating tongue or ice shelf is permitted when the ice thickness is less than
 265 the flotation thickness. A simple implementation of submarine melting is applied both at the
 266 grounding line and where ice is floating, decreasing the ice thickness by a fixed amount for all
 267 grid points between the grounding line and the calving front. A moving model grid, for which
 268 the horizontal grid spacing adjusts at each time step to accommodate the new glacier length, is
 269 used to allow for continuous tracking of the grounding line position (Vieli and Payne, 2005).
 270 Values for constants and physical parameters used in the model are given in table 1.
 271

272
 273
 274
 275
 276

277 **3.2 Model inputs**

278
279 The ice stream bed profile was extracted along the flowline (figure 1) at 500 m horizontal
280 intervals, with present day bathymetric values obtained from the Baltic Sea Bathymetry
281 Database (Baltic Sea Hydrographic Commission, 2013) and topographic values from
282 available 50 m gridded elevation data (Lantmäteriet, 2015). Given the high local topographic
283 variability of the bed, spline smoothing was applied to avoid including features
284 unrepresentative of the bay-wide basal topography. The central flowline elevation profile was
285 used in modelling, rather than width-averaged elevation, due to uncertainty in prescribing the
286 width of the ice stream and clear data constraint on the central pathway.

287
288 To account for bed isostatic evolution and sea level forcing throughout the model period (11.6
289 – 9.65 ka BP), we use empirically derived relative sea level (RSL) reconstructions that span
290 the operational length of the Bothnian Sea Ice Stream. Shoreline displacement data from sites
291 in Norrbotten (Lindén et al., 2006), Ångermanland (Berglund, 2004), Gästrikland (Berglund,
292 2005) and Södertörn (Hedenström and Risberg, 1999) were selected accordingly (figure 1).
293 The published ^{14}C ages for the isolation of lake basins at each site were converted to calendar
294 years B.P. using the IntCal13 calibration curve (Reimer et al., 2013). 2nd or 3rd degree
295 polynomials were applied to interpolate between the calibrated dates for each site and
296 generate a local RSL curve with a temporal resolution of 10 years. A spline was then fitted to
297 the four shore displacement values at each time step to generate an evolving RSL model that
298 is appropriate in both time and space at each step along our flowline (figure 2).

299
300 The spatial distribution of an initial surface mass balance was chosen to reflect the colder and
301 drier conditions of the Younger Dryas (Carlson, 2013; Muschitiello et al., 2015). We applied
302 a surface mass balance that varies linearly with elevation, ranging from $-0.5 \text{ m a}^{-1} \text{ m}^{-2}$ at sea
303 level up to a fixed maximum of $0.25 \text{ m a}^{-1} \text{ m}^{-2}$ at 1000 m a.s.l., with an associated equilibrium
304 line altitude (ELA) of 665 m a.s.l.. This is broadly comparable with reconstructed Younger
305 Dryas gradients for northern Norway described in Rea and Evans (2007).

306
307 With this set-up, we investigated atmospheric and marine forcings on the catchment via four
308 model mechanisms: relative sea level at the grounding line, increasingly negative surface
309 mass balance (reduction of ice thickness across the surface profile), increasing the depth to
310 which surface meltwater fills crevasses (hydrofracture trigger), and increasing submarine melt
311 (reduction of ice thickness across the floating portion).

312

313 **3.3 Model experiments**

314 The model was spun up to an initial stable, late Younger Dryas position consistent with the
315 11.6 ka BP marginal position presented in Stroeven et al. (2016). This steady state
316 configuration, from which all perturbation experiments were initialised, was produced with
317 sea level held constant at spatially-interpolated values for 11.6 ka BP, a constant crevasse
318 water depth of 95 m (47% of the steady state terminus thickness), an average of the maximum
319 and minimum ice stream widths (figure 1), and no submarine melting. The surface mass
320 balance was initially set at $0.2 \text{ m a}^{-1} \text{ m}^{-2}$ across the full length of the profile for 1500 years to
321 allow for the growth and evolution of an ice surface with a realistic slope profile. A surface
322 mass balance varying linearly with elevation, as described above, was then applied and the
323 model was run until the ice surface had stopped evolving after 6500 years. Thereafter, our
324 model experiments were run for a period of 2 kyr, reflecting the time between the late

325 Younger Dryas and full deglaciation as described by Stroeven et al. (2016). Four sets of
326 experiments, a total of 75 runs, were conducted as described in table 2, designed to explore
327 the sensitivity of ice flow behaviour and retreat rates to (i) system geometry, (ii) atmospheric
328 forcings, (iii) marine forcings, and (iv) combined forcings. In each case, the initial variable
329 values were held at those used in the spin up (as above).

330
331 Each model run is named in accordance with the following nomenclature. The code prefix
332 indicates the type of forcing applied, whereby BT: bed tilt, ISW: ice stream width, SMB:
333 surface mass balance, CWD: crevasse water depth, SM: submarine melt and BF: basal
334 friction. In the case of model geometry (BT and ISW), the suffix indicates the deviation from
335 the standard geometry, expressed as a percentage, and for BF the suffix indicates the fraction
336 of full basal friction (=1.0). For SMB, CWD and SM, each in their respective units, the suffix
337 indicates the rate of change of the forcing per 500 years (Table 2). The default run set-up for
338 SMB, CWD and SM is a linearly applied forcing; experiments using step-changes include the
339 term 'step' in the suffix. Following this scheme, experiment SMB_step040 denotes forcing
340 the model with surface mass balance (holding all other parameters at their default/initial
341 value), applied in a step-wise fashion with a change of $-0.4 \text{ m a}^{-1} \text{ m}^{-2}$ every 500 years to a
342 final magnitude of $-1.7 \text{ m a}^{-1} \text{ m}^{-2}$.

343
344 The first set of experiments was designed to test sensitivity to topography and geometry,
345 including the isostatic adjustment of the topography manifest in our RSL model. An initial
346 experiment forced retreat solely with *RSL change*, holding other variables constant; an
347 additional test of RSL sensitivity removed the RSL forcing from a standard (surface mass
348 balance forced) model run with default catchment geometry. Thereafter, sensitivity testing to
349 both *bed tilting* and *ice stream width* was investigated, using the same surface mass balance
350 forced run (SMB_040) as a control. Theory dictates that bed depth, and thus slope, is a strong
351 control on the rapidity of ice stream retreat and grounding line stability (Weertman, 1974;
352 Schoof, 2007). While the spatially non-linear isostatic rebound in Scandinavia (cf.
353 Hedenström and Risberg, 1999; Berglund, 2004) is accounted for in our RSL adjustment,
354 there are uncertainties inherent in radiocarbon dating and calibration of samples used to infer
355 RSL history, and further errors are likely introduced in interpolating between sites. Sensitivity
356 testing to bed tilt was implemented by increasing the slope of our RSL-adjusted bed
357 topography by 10% and 20%. We explore sensitivity of the model to the defined catchment
358 width by increasing and decreasing the average flow path width (model default) by 25 and 50
359 % to cover the drawn extent of maximum and minimum ice stream boundaries.

360
361 The influence of atmospheric warming and ice surface melting is investigated via changes in
362 *surface mass balance* and *crevasse water depth* in the second set of experiments. For both we
363 test the response to linearly increasing forcings, and step-wise changes in forcing. Surface
364 mass balance is applied along the flowline, forcing evolution of the ice surface in combination
365 with ice flux and changes in ice stream width (equation 3). Crevasse water depth is
366 implemented as d_w in equation 5, whereby increasing crevasse water depth allows for deeper
367 propagation of surface crevasses via hydrofracture, and the possibility for increased calving.
368 Crevasse water depth is a poorly constrained absolute value and in this implementation should
369 not be treated as a real value, but rather a tuning parameter linked to a physical mechanism.
370 An initial water depth of 95 m produces a stable spin-up state, so we begin increasing values
371 from here. Linear forcing experiments impose a steady yearly increase, while step change
372 experiments apply the specified forcing once every 500 years (table 2). For CWD, values
373 increase from an initial 95 m to an end-of-run value ranging from 115 (CWD_5) to 215 m
374 (CWD_30). In the case of SMB, surface mass balance at sea level decreases from an initial

375 value of $-0.5 \text{ m a}^{-1} \text{ m}^{-2}$ to a final value ranging from -0.9 (SMB_010) up to $-4.1 \text{ m a}^{-1} \text{ m}^{-2}$
376 (SMB_090) by the end of the model run, representative of the most negative values of surface
377 mass balance at the margin of the contemporary Greenland Ice Sheet (Ettema et al., 2009).

378
379 In the third set of experiments, end-of-run rates of *submarine melt* from 8 (SM_2) to 1000 m
380 a^{-1} (SM_250) are investigated, providing a range representative of subaqueous melting
381 observed for freshwater-terminating glaciers (Hochstein et al., 1998) up to the largest order of
382 magnitude in submarine melt rates documented for the present day Greenland Ice Sheet
383 (Rignot et al., 2010; Enderlin and Howat, 2013). Linear and step-changes in submarine
384 melting are investigated (table 2), as described for experiment set 2.

385
386 The fourth set of experiments combines multiple forcings of crevasse water depth, surface
387 mass balance, and submarine melting. Paired forcing combinations for selected values of
388 linear change are used to investigate the effect of multiple forcings on the rapidity of retreat,
389 and to better illustrate the *relative* sensitivity of ice stream dynamics to each of the paired
390 forcings. Finally, since the above described experiments only address the impact of increased
391 melting on surface and englacial processes, a brief investigation of meltwater-enhanced basal
392 sliding is also conducted. A triple combination of forcings is applied for this purpose, using
393 low-to-moderate end-of-run maximum values of crevasse water depth (135 m), surface mass
394 balance ($-1.7 \text{ m a}^{-1} \text{ m}^{-2}$), and submarine melt (20 m a^{-1}). A basal sliding enhancement was
395 imposed 1000 years into the model runs, reducing the *basal friction* parameter, μ , in equation
396 1, by 20 % and 30 % (CWD10_SMB030_SM5_BF08 and CWD10_SMB030_SM5_BF07
397 respectively). A control run with full basal friction (CWD10_SMB030_SM5_BF1) is
398 conducted for comparison.

399

400

401 **4. Results**

402

403 ***4.1 Sensitivity to system geometry: sea level, topography and catchment width***

404 Forcing the model with RSL change alone produced only a very small retreat of the grounding
405 line of c.21 km over 2000 years (figure 2), suggesting that it is unlikely that sea level alone
406 could force grounding line retreat from a stable Younger Dryas position. Accordingly, further
407 sensitivity testing to catchment geometry used surface mass balance run SMB_040 as a
408 control against which to compare modelled response. An initial run in which we remove the
409 RSL forcing further confirms that modelled Bothnian Sea deglaciation is only weakly
410 sensitive to sea level, with the total grounding line retreat distance deviating by only 9.3 %
411 between runs with and without RSL change.

412

413 Grounding line retreat for experiments in which ice stream width was increased and decreased
414 by 25% and 50 % deviated very little from control run SMB_040 (figure 2). The final
415 grounding line positions for these four experiments, at 9.65 ka BP, ranged between 500 m and
416 18 km from that of SMB_040, between 2.95 and 0.08 % of the total retreat distance.
417 Experiments for decreased width produced the largest, although still small, deviation from the
418 control. These results convey a relative insensitivity to changes in ice stream width within the
419 minimum and maximum range as drawn in figure 1, such that any error in defining the
420 average width for use in subsequent sensitivity tests is assumed to not significantly affect
421 modelled retreat rates. Enhancing tilt of the bed via a 10 and 20 % increase in slope in the
422 direction of the ice divide resulted in final grounding line positions exceeding run SMB_040

423 by 2 km and 57 km respectively (figure 2), with considerably less spatial variability preceding
424 the very end of the model run. This amounts to between 0.34 and 9.35 % of the total retreat
425 distance, with the grounding line reaching the final position of the surface mass balance-
426 driven control run c.50 and c.100 years earlier. In this setting, therefore, the modelled ice
427 stream exhibits relatively little sensitivity to width and bed tilt. We can thus be reasonably
428 confident that the results of our following analyses, which all adopt the control run geometry,
429 will represent the major controls on deglaciation.

430

431

432 **4.2 Sensitivity to atmospheric and submarine melting**

433 *4.2.1 Individual forcings*

434 The modelled response of the grounding line position to linear and stepwise changes in
435 crevasse water depth, surface mass balance and submarine melting are illustrated in figure 3.
436 The application of sufficiently large individual linear forcings of both crevasse water depth
437 (175 m or more by the end of the run) and surface mass balance ($-3.1 \text{ m a}^{-1} \text{ m}^{-2}$ or more by the
438 end of the run) result in full retreat of the entire flowline by the end of the model period
439 (figure 3A and C), and all three forcing mechanisms are individually capable of driving retreat
440 of ice out of the present-day Gulf of Bothnia. While we note that the upper portion of the
441 flowline is not, strictly, appropriate for the known local retreat geometry and timing, we
442 report here on the *relative* patterns of retreat produced by the different forcing mechanisms
443 over the present-day marine portion of the flowline, whose geometry is well-constrained.

444

445 Over the main portion of the trunk of the Bothnian Sea (i.e. c. 430 – 700 km along flowline)
446 the modelled retreat rate is rather insensitive to the magnitude of crevasse propagation, when
447 this is forced by a linearly increasing crevasse water depth. The slope of the plotted retreat
448 trajectories in figure 3A is consistent between model runs. The magnitude of crevasse
449 instead determines how long the grounding line pauses at particular locations, and therefore
450 controls the absolute timing of retreat rather than the rate. Higher rates of crevasse
451 propagation succeed in driving retreat of the grounding line to the Härnösand Deep (c. 400
452 km along flowline) within our modelled timeframe, at which point runaway deglaciation
453 faster than the deglacial chronology of Stroeven et al. (2016) is triggered. Stepped forcing in
454 crevasse propagation, in contrast, produces rather different retreat trajectories depending on
455 the magnitude of the forcing (figure 3B).

456

457 In contrast to crevasse propagation, increasing the magnitude of the surface mass balance
458 forcing steadily accelerates the rate of grounding line retreat (figure 3C). Runs with
459 increasingly negative surface mass balance exhibit less local variability in retreat rate, with
460 fewer and less pronounced inflections in the plotted retreat trajectories under more negative
461 surface mass balance scenarios. Surface mass balance in excess of $-1.9 \text{ m a}^{-1} \text{ m}^{-2}$ (SMB_035)
462 at the end-of-run is required to drive the grounding line out of the present-day Bothnian Sea,
463 while compared to the known deglacial chronology (figure 1), surface mass balance scenarios
464 of -3.1 to $-4.1 \text{ m a}^{-1} \text{ m}^{-2}$ (SMB_065 and SMB_090) by the end of the run achieve full
465 deglaciation within an appropriate time frame.

466

467 Submarine melt-forced retreat of the ice stream results in relatively little grounding line
468 response to end of run values of up to 100 m a^{-1} (SM_25) (figure 3E). Only exceptionally high
469 submarine melt rates (200 m a^{-1} or more) can force complete retreat of this catchment to the
470 terrestrial environment.

471

472 Figure 4 illustrates the evolution of the ice surface profile and ice flow velocity for selected
473 individual linear forcings of crevasse water depth, surface mass balance, and submarine
474 melting. These three experiments retreat to, or close to the prescribed ice divide over the 2000
475 year model run, with experiment CWD_20, with a maximum water depth of 175 m, fully
476 deglaciating within the final 50 year timestep under very rapid retreat. Terminus retreat forced
477 by an increase in crevasse water depth is characterised by two periods of relative retreat
478 slowdown (figure 4A) coinciding with a reduction in ice surface velocities (figure 4D), both
479 of which fall on a gentle reverse bed slope just prior to its abrupt steepening. The first occurs
480 at c.720 km from the ice divide and the second at c. 450 km from the ice divide. This
481 pronounced deceleration in the rate of grounding line retreat coincides with a narrowing of the
482 ice stream width, but is seen only in runs for which crevasse water depth is the sole, or one of
483 two applied forcings (figure 3A, B; figure 5A, C), and not when the model is forced by a
484 change in submarine melting or surface mass balance alone. Immediately preceding full
485 deglaciation in the final timestep of run CWD_20 there is a large peak in ice surface velocity,
486 reaching c. 6000 m a⁻¹ (figure 4D). This rapid retreat in the final 50 years could be attributable
487 to a debuitressing effect caused by loss of the ice shelf in the final timestep, to a reduction in
488 basal and/or lateral drag, or to acceleration of ice surface velocities in response to a
489 steepening ice surface profile. When forced by decreasing surface mass balance alone, the ice
490 stream surface profile lowers at a considerably greater rate than when forced by crevasse
491 water depth or submarine melting (figure 4B). The decreasing mass balance and thus ice flux
492 leads to a reduction in ice surface velocities along the flowline, and without additional
493 increases in calving or submarine melt, a large floating ice tongue can form, stretching up to
494 c.100 km in length. Grounding line retreat forced by submarine melt alone (figure 4C) is
495 steady in comparison to crevasse water depth-forced retreat, with less variation in ice surface
496 velocities (Figure 4F), and no major periods of retreat slowdown.

497

498 The application of linearly-increasing forcings results in retreat rates which are non-linear.
499 This indicates sensitivity of grounding line retreat to local changes in basal topography. There
500 are consistent inflections in the grounding line responses of many of the model runs, including
501 at c.780, 745, 720, 625, and 485 km along the flowline, which correspond to abrupt changes
502 in local basal slope (figure 3). These bed topography changes therefore appear to control
503 small-scale grounding line responses regardless of the mode of 'external' applied forcing.
504 Step-wise forcing experiments, in which larger increases were imposed every 500 years to
505 investigate response to abrupt forcings, yield a grounding line response which only
506 occasionally responds in a step-wise fashion. Response to step changes is most pronounced
507 for crevasse water depth experiments CWD_step20 and CWD_step30 (figure 3B), where
508 acceleration in grounding line retreat is enhanced following step increases at 10.6 and 10.1 ka
509 BP. Local variation in retreat rates is subdued during these step-driven periods of rapid
510 retreat, suggesting that while the modelled ice stream is adapting to these sudden changes, the
511 influence of local topography is overridden by other controls. Neither surface mass balance
512 nor submarine melting rates drive any abrupt retreat events at the times when an abrupt
513 (stepped) forcing is applied. In the case of the former this may be due to surface mass balance
514 having a time-integrated effect, thus an abrupt reduction in surface mass balance may not
515 have an instantaneous effect on the grounding line position.

516

517 The above results indicate that individual forcings, if they are sufficiently large, can lead to
518 full retreat by the end of the model period. These results also demonstrate that while sufficient
519 step-changes in crevasse propagation via increasing crevasse water storage forces acceleration

520 of retreat rates, this response is short-lived. Within our suite of model experiments, step
521 changes in individually applied forcings do not, alone, cause a catastrophic deglaciation event.
522

523 *4.2.2 Paired forcings*

524 Each forcing mechanism can drive complete retreat of the modelled Bothnian Sea flow path if
525 its magnitude is sufficiently high. It is instructive, therefore, to examine paired forcing
526 combinations, to allow the *relative* influence of crevasse water depth, surface mass balance
527 and submarine melting on retreat trajectories to be evaluated more closely. Figure 5 illustrates
528 grounding line retreat for each combination of forcings, where forcings are kept low to
529 moderate in magnitude (table 2) in order to allow us to best judge sensitivity without one
530 signal artificially overriding another. Individually none of these modest forcings would cause
531 retreat to more than c. 500 km from the ice divide after 2000 years (central Bothnian Sea), but
532 in certain combinations they amount to full or close-to-full retreat. The most striking result of
533 pairing forcings is that the effects of submarine melt are negligible. Figure 5A shows that
534 crevasse water depth exerts a substantially greater control on modelled grounding line retreat
535 than submarine melting. Grounding line retreat trajectories cluster tightly according to the
536 magnitude of crevasse water depth, while varying the submarine melt rate has very little
537 effect. Only experiment CWD15_SM10 exhibits notable retreat of the final grounding line
538 position in response to increased submarine melting, and this is clearly coincident with a steep
539 reverse bed slope. While runs pairing surface mass balance and submarine melt do not exhibit
540 the same tight clustering of retreat trajectories, these responses plot in an order dictated by
541 surface mass balance magnitudes (figure 5B), and therefore we interpret the surface mass
542 balance forcing to similarly dominate over submarine melting. In contrast, it is difficult to
543 separate the relative influence of crevasse water depth and surface mass balance (figure 5C).
544 Grounding line retreat trajectories cross-cut one another and neither mechanism appears to
545 dominate. We note that our greatest (most negative) surface mass balance forcing of -0.3 m a^{-1}
546 m^{-2} over 500 years ($-1.7 \text{ m a}^{-1} \text{ m}^{-2}$ by end-of-run) drives more rapid and extensive retreat than
547 an increase in crevasse water depth in combination with smaller changes in surface mass
548 balance. It is apparent, however, that within the magnitudes of forcings explored here, surface
549 melt-related processes dominate over submarine melting in driving grounding line retreat in
550 the Bothnian Sea.

551

552

553 *4.2.3 Full forcing and sensitivity to basal friction*

554

555 While enhanced surface melting appears to be an important driver of ice retreat in the
556 Bothnian basin, we have thus far only considered its effect via surface mass balance reduction
557 and surface crevasse propagation. Surface melting is not physically coupled within the model
558 to any basal sliding response mechanism. Reducing basal friction allows for a simple
559 investigation of the possible influence of increased surface meltwater production and delivery
560 to the subglacial domain. Three final multiple forcing experiments were conducted with a
561 fully combined (triple) forcing set-up, comprising a control run with baseline basal friction,
562 and two runs with reduced basal friction (figure 6). With the baseline basal friction (i.e. as in
563 all previous simulations), the combination of forcings yields a pattern of margin retreat that
564 sticks persistently over the Åland sill (c.720 km), pauses again at c.600-620 km and thereafter
565 the retreat rate increases. The accompanying ice velocities, which peak initially c.670 km
566 from the ice divide immediately following rapid retreat over the deep water of the Åland Sea,
567 are reduced to moderate-fast flow speeds through the central Bothnian Sea, and rise again as

568 the retreat rate increases over the reverse bed and deep basin of Hårnösandsdjupet (c. 500-350
569 km) (figure 6, A and D). We find that a 20 and 30 % reduction in basal friction does not
570 significantly alter either the spatial pattern of retreat, or the magnitude of grounding line
571 retreat accomplished in 2000 years, though increases some minor spatial variability (i.e.
572 standstills and retreat steps). Absolute ice flow velocities increase with the reduction in basal
573 friction, particularly between c. 600 and 670 km, but the spatial pattern of velocity evolution
574 is similarly insensitive to basal friction.

575

576

577 **5. Discussion**

578

579 The results described above indicate that each individual mechanism could lead to complete
580 or close to complete retreat if the applied forcing is sufficient. However, it is likely that such
581 values may become unreasonable in order to achieve this. We designed the range of
582 experimental values according to those reported in both/either contemporary or palaeo
583 settings, specifically to meet our sensitivity testing objectives, but it does not follow that this
584 range should be applicable to the case of the Bothnian Sea. This applies particularly to
585 submarine melting, for which even a melt rate of 1000 m a^{-1} , albeit through a very simple
586 implementation, does not result in full retreat of the ice stream (figure 3E). While such
587 magnitude of submarine melting may be applicable to particular individual outlets of the
588 present day Greenland Ice Sheet (Rignot et al., 2010; Enderlin and Howat, 2013), it is an
589 exceptionally high rate compared to other Greenland and Antarctic catchments (Jacobs et al.,
590 2011; Enderlin and Howat, 2013; Rignot et al., 2013) and it is highly unlikely that melting of
591 this extent was active in the Gulf of Bothnia given that climate was likely still cooler than
592 present during deglaciation.

593

594 During the time period of Bothnian Sea deglaciation (c. 11.6-10.3 ka), exchange of Baltic-
595 Bothnian waters with the North Sea was extremely limited, confined to the ever-shallowing
596 and narrowing Närke Strait across central Sweden as land uplift proceeded to close the basin
597 outlet (Yoldia Sea to Ancylus Lake transition: Björck, 1995; Andrén et al., 2011). Limited
598 marine inflow created a brackish environment for a maximum of c.300 years 11.4-11.1 ka
599 (Andrén et al., 2011); otherwise, the Bothnian Sea was a freshwater body fed by cold glacial
600 meltwater. Without proglacial circulation driven by either water mass exchange or plume-
601 driven convection (Jenkins, 2011), we expect low transfer of heat from the proglacial water
602 body to the ice front, and therefore very low melt rates. In the range of values that are realistic
603 in this setting, we conclude from our model responses that it is likely that the Bothnian Sea
604 Ice Stream was relatively insensitive to submarine melting. Through quantitative analysis of
605 mass loss partitioning for the triple forcing experiment (figure 6A), it is clear that the
606 contribution of submarine melting to overall mass loss is relatively small in comparison to
607 surface mass balance and calving (figure 7). However, while absolute contribution to mass
608 loss is low, small peaks in submarine melting precede some large calving-driven retreat
609 episodes in this experiment, suggesting it may have a more important role in triggering retreat
610 from topographic pinning points.

611

612 Our sensitivity tests to bed geometry revealed that retreat of this ice sheet sector was likely
613 relatively insensitive to RSL change and associated isostatic adjustment. This insensitivity of
614 modelled grounding line retreat to either submarine melting or RSL change indicate that this
615 marine ice sheet sector was governed only minimally by direct marine processes. Conversely,
616 the modelled grounding line retreat of the Bothnian Sea Ice Stream is shown to be highly
617 sensitive to surface melting, which acts both through enhanced crevasse propagation due to

618 increased water infilling of surface crevasses (i.e. hydrofracture), and through an increasingly
619 negative surface mass balance and associated thinning of the ice surface profile. We cannot
620 presently separate the influence of surface mass balance and crevasse propagation.
621 Qualitatively, crevasse water depth appears to affect the timing of retreat more than the rate,
622 via control on the duration of episodes where the grounding line appears to undergo limited
623 movement. Surface mass balance affects retreat rates in a steadier fashion. A large negative
624 surface mass balance (end-of-run values of -3.1 to -4.1 $\text{m a}^{-1} \text{m}^{-2}$) is independently capable of
625 driving complete Bothnian Sea retreat within a timeframe matching the terrestrial clay varve
626 chronology for deglaciation (Stroeven et al., 2016). Such surface mass balance rates are in
627 fact rather moderate compared to an estimated -5 to -9 $\text{m a}^{-1} \text{m}^{-2}$ for the southern Laurentide
628 Ice Sheet during early Holocene (Carlson et al., 2009), and the geomorphological record
629 exhibits abundant evidence of high discharge, well-connected subglacial meltwater drainage
630 (Greenwood et al., in press). Implementation of step-wise reductions in surface mass balance,
631 however, did not drive instantaneous response or catastrophic retreat, possibly due to the
632 time-integrated effect of surface mass balance (Figure 3D). Widespread basal crevasse
633 squeeze ridges additionally point to a highly fractured ice body, likely vulnerable to surface-
634 melt enhanced hydrofracture. While we cannot yet quantitatively disentangle mass balance
635 and hydrofracture effects on retreat rate, our model implicates ice surface melting in driving
636 deglaciation, as illustrated by its contribution to overall mass loss (figure 7).

637
638 Increased melting and increased crevasse propagation are closely linked on contemporary ice
639 sheets (Clason et al., 2015), and collectively act as triggers for secondary forcings including
640 increased calving and ice cliff failure (Benn et al., 2007; Pollard et al., 2015; Colgan et al.,
641 2016), and changes in efficiency of the subglacial hydrological system (Cowton et al., 2013;
642 Mayaud et al., 2014). The extent to which increased surface-to-bed meltwater transfer
643 influences annual ice surface velocities remains contentious, and the extent to which increased
644 efficiency of the subglacial drainage system may offset enhanced basal lubrication on the
645 Greenland Ice Sheet remains uncertain (Sundal et al., 2011; Sole et al., 2013; van de Wal et
646 al., 2015). Given the likely importance of meltwater in the Bothnian Sea system, we
647 employed a simple proxy for meltwater-enhanced sliding to allow for a first-order exploration
648 of the possible effects on ice dynamics and retreat. While reducing basal friction did result in
649 increased velocities along the flowline overall, it did not produce any significant variation in
650 the spatial pattern of velocities along the flowline. Additionally, we do not observe any
651 differences in the overall duration of deglaciation, despite higher velocities accompanying
652 low friction; the velocity response, in itself, does not make the system any more vulnerable to
653 rapid retreat. In this setting, enhanced flow rates are offset by an enhanced duration of
654 grounding line pinning at those localities prone to grounding line retreat slowdown (Figure 6).

655
656 Consistent areas of grounding line retreat slowdown and of increased retreat rates are
657 produced across the suite of model experiments. We interpret this pattern to indicate model
658 sensitivity to local variations in basal topography and ice stream width, despite the relative
659 insensitivity to the absolute magnitude of these factors at the catchment scale (figure 2).
660 Under almost all forcings applied in this study the margin retreat slows $c.720$ km along the
661 flowline for a short period of $c.250$ years, immediately preceding rapid retreat of $c.50$ km
662 within 50 years through an area of deep water in the Sea of Åland. Grounding line retreat
663 slowdown also occurs at $c.450$ km along flow, on the gentle reverse slope distal to the
664 Hårnösand Deep, most commonly and markedly when crevasse propagation is part of the
665 applied forcing. This is clearly the case in both single and paired forcing runs (Figs 3-5),
666 though the full forcing scenario only displays a brief ($c. 50$ year) slowdown of retreat under
667 the enhanced basal sliding scenario in figure 6C. In the full forcing run and in the paired

668 CWD-SMB forcing, there is a phase of markedly reduced retreat rate c.650-600 km along
669 flowline.

670

671 The geomorphological and geological record of the Bothnian Sea identifies *i*) a palaeo-ice
672 stream pathway, with high ice flow velocities limited to a stretch approximately 250 – 620 km
673 along our modelled flowline, *ii*) the terminal zone of the active ice stream, located in the
674 central-southern Bothnian Sea c.600-620 km along flowline (figure 6G), *iii*) a zone of
675 relatively enhanced basal stability immediately south of the Härnösand Deep (figure 1), and
676 *iv*) a 5-30 m thick sequence of glacial sediments in the main trunk of the Bothnian Sea, while
677 the distal end of our flowline (from c. 660 km) passes over crystalline bedrock with only a
678 thin (< 10 m) sediment cover. The modelled positions of slowdowns in grounding line retreat,
679 and the general *lack* of evidence for prolonged periods of retreat slowdown through the
680 Bothnian Sea, are consistent with these properties. The first modelled position of minor
681 slowdown, across the Åland shallows, occurs on the crystalline substrate where increased bed
682 roughness may be expected to locally reduce ice flow velocities and stabilise the grounding
683 line (Rippin et al., 2011; Livingstone et al., 2012), and where small glacial lineations are only
684 weakly developed. Additionally, this position coincides with a narrowing of the ice stream
685 width (figure 1), which is reported elsewhere to permit a slowdown of retreat even on reverse
686 bed slopes (Jamieson et al., 2012; Gudmundsson et al., 2012). The island of Åland itself has,
687 in the past, been proposed as a “sticky spot” (Holmlund and Fastook, 1993), acting to inhibit
688 ice flux through the south-central sector of the FIS, which has led to overly-rapid retreat in
689 previous modelling studies (Clason et al., 2014). Slowdown of retreat c.450 km along
690 flowline, just south of Härnösand Deep, emerges consistently from our model runs and is also
691 indicated by the appearance of transverse wedge-like ridges superimposed on MSGs
692 (Greenwood et al., in press) and which record a zone of reduced flow and margin stability
693 after a period of ice streaming. Since modelled grounding line retreat only slows across this
694 zone when surface crevasse propagation is a component of the forcing, we implicate enhanced
695 crevasse propagation as a control on stability in this system. Deeper crevasses lead to an increase in
696 calving, maintaining a steep ice sheet profile and restricting formation of a floating tongue,
697 resulting in a grounding line that is more resistant to buoyancy and thus potentially more
698 likely to stabilise over reverse bed slopes.

699

700 With paired atmospheric forcings (surface mass balance and crevasse water depth) and with a
701 fully combined (triple) forcing, but notably in none of the individual forcings nor the
702 alternative pairs, the model predicts a prominent zone of grounding line retreat slowdown at c.
703 650-600 km along flowline, which lasts for 200-250 years. This is consistent with the
704 geomorphological record, which reveals the terminal zone of the Bothnian Sea Ice Stream at
705 c.620-600 km (figure 6G). In this zone, sets of MSGs cross-cut sub-parallel to one another,
706 in contrast to further up the ice stream trunk where lineations display a high degree of parallel
707 conformity (e.g. figure 1D). While there is no evidence for a grounding zone wedge or other
708 ice-marginal deposits here, the lineation overprinting requires that there was a persistent ice
709 stream terminus at c.620-600 km, maintaining its position for sufficient time to allow the
710 marginal flow direction to shift back and forth a few degrees. Our modelling supports this
711 central-southern Bothnian Sea position of a moderately stable grounding line, and its
712 appearance in only the atmospherically-forced runs again attests to the likely importance of
713 ice surface processes in governing this ice sheet sector.

714

715 The patterns of ice velocity evolution, on the other hand, are an imperfect match to the
716 reconstruction of ice streaming from the glacial landform record. That there is only an MSG
717 record of ice streaming up to 620 km along our flowline, beyond which lies a separate group

718 of small (often bedrock) drumlins and crag and tails with a flow direction offset from the
719 MSGs, suggests that ice streaming occurred as a distinct event once retreat into the Bothnian
720 Sea had already begun. Furthermore, this ice stream event did not extend the full length of the
721 Bothnian Sea (Greenwood et al., in press). We would therefore expect to see initially low
722 flow velocities, with an abrupt shift to high velocities once the margin reached c. 620 km.
723 Modelled flow velocities, in contrast, peak immediately upon withdrawal from the Åland Sea,
724 at c. 680-690 km, and then decline towards 600 km, although still at rates typical of ice
725 streaming, i.e. 500-1000 m a⁻¹. Modelled velocities peak again around 500 km along flowline,
726 in the central Bothnian Sea, which is coincident with where the length of MSGs reach their
727 peak.

728

729 In its present form the model does not capture the Bothnian Sea Ice Stream as an ‘event’
730 which abruptly activates during the Bothnian Sea deglaciation, or the precise timing of
731 southern FIS deglaciation known from the terrestrial clay varve chronologies (summarised in
732 Stroeven et al., 2016). However, our present implementation of atmospheric and marine
733 drivers is designed only to test sensitivity to retreat triggers, and we conclude that it is likely
734 that the ice streaming event did not arise simply as a non-linear response to steady climate
735 amelioration. Our model experiments highlight surface melting as an important control on
736 Bothnian Sea grounding line retreat. Despite limitations associated with a one-dimensional
737 model, our results shed new light upon the mode of marine-based ice sheet retreat in the
738 southern FIS and, by extension, other low-relief terrains associated with large, proglacial
739 water bodies. That the Bothnian Sea Ice Stream is a calving ice stream that most likely
740 collapsed without significant sensitivity to marine forcing (i.e. sea level change and
741 submarine melting) highlights the need to considerably improve our understanding of how
742 subaqueous ice sheet sectors respond to both atmospheric and marine forcings.

743

744

745 **6. Conclusions**

746

747 We applied a well-established flowline model to the case of the Bothnian Sea Ice Stream,
748 validated against geomorphological evidence that has been mapped and analysed from
749 recently-collected high resolution bathymetric data. Results of sensitivity testing to both
750 single and multiple forcings of crevasse water depth, surface mass balance, and submarine
751 melting point toward retreat governed largely by increased surface meltwater production in
752 response to climatic changes following the Younger Dryas. Submarine melting and relative
753 sea level change are found to have only minimal effect on grounding line retreat in our
754 simulation. We thus highlight the Bothnian Sea as a case where despite the marine setting,
755 retreat of this large ice sheet sector was likely governed primarily by atmospheric, rather than
756 marine processes. While the modelling presented here applies very simple implementations of
757 calving, surface and submarine melting, our results stress the importance of better
758 understanding the multitude of responses to climatic and environmental controls exhibited by
759 marine-terminating ice sheets.

760

761 Our suite of model experiments indicates no major standstills after the Younger Dryas, but
762 short-lived periods of grounding line retreat slowdown and of accelerated retreat. The
763 locations of slowdowns are consistent with the geomorphological record, and are interpreted
764 to indicate sensitivity to local variations in basal topography and in ice stream width. While
765 the relative influence of meltwater-forced crevasse propagation and surface mass balance
766 cannot yet be separated, we find that the modelled fit with the geomorphological record of
767 grounding line stabilisation is strongest when both processes are fully incorporated. The

768 model does not replicate the activation of the Bothnian Sea Ice Stream as a discrete, fast-flow
769 event that is triggered once retreat is already underway. Since activation does not arise from
770 either linearly or regularly stepped increases in forcing, we infer the ice stream may have
771 switched on in response to a specific event-forcing not accounted for in our current modelling
772 set-up. Implementation of a realistic palaeo-climate forcing is necessary to evaluate the
773 temporal and spatial response of the Bothnian Sea Ice Stream to climatic variations under a
774 period of rapid environmental change. The availability of high resolution topographic and
775 bathymetric data in this region, in concert with geomorphologically-validated numerical
776 modelling, provides a unique opportunity to improve our understanding of ice stream
777 dynamics and collapse in a major basin of the Fennoscandian Ice Sheet, until now a gap in the
778 deglacial history of the region.

779

780

781 **Acknowledgements and Data**

782

783 We gratefully acknowledge the financial support of the Swedish Radiation Safety Authority
784 (PH), the Carl Trygger Foundation for Scientific Research (CCC), the Geological Survey of
785 Sweden, and the Swedish Research Council (SLG). The contribution of JML was partly
786 supported by FORMAS grant 2013-1600. The Swedish Maritime Administration and the
787 Geological Survey of Sweden kindly provided access to geomorphological and geological
788 data. Bathymetric and topographic data can be accessed via the Baltic Sea Bathymetry
789 Database (<http://www.bshc.pro/>) and Lantmäteriet (<http://www.lantmateriet.se/>) respectively.
790 We wish to thank Francesco Muschitiello and Arjen Stroeven for discussions which helped to
791 improve the study. We also thank Nick Golledge, Olga Sergienko and an anonymous reviewer
792 for their helpful comments.

793

794

795 **References**

796 Anandakrishnan, S., Voigt, D.E., Alley, R.B. and King, M.A., (2003), Ice stream D flow
797 speed is strongly modulated by the tide beneath the Ross Ice Shelf, *Geophys. Res. Lett.*, 30,
798 doi:doi:10.1029/2002GL016329

799

800 Andrén, E., Andrén, T. and Sohlenius, G., (2000), The Holocene history of the southwestern
801 Baltic Sea as reflected in a sediment core from the Bornholm Basin, *Boreas*, 29, 233-250

802

803 Andrén, T., Björck, S., Andrén, E., Conley, D., Zillén, L. and Anjar, J., (2011), The
804 development of the Baltic Sea Basin during the last 130ka, in Harff, J., Björck, S. and Hoth,
805 P., *The Baltic Sea Basin*, Springer Berlin Heidelberg, pp. 75-97.

806

807 Arnold, N. and Sharp, M., (2002), Flow variability in the Scandinavian ice sheet: modelling
808 the coupling between ice sheet flow and hydrology, *Quaternary Sci. Rev.*, 21, 485-502

809

810 Baltic Sea Hydrographic Commission, (2013), Baltic Sea Bathymetry Database version 0.9.3.
811 Downloaded from <http://data.bshc.pro/> on 11/03/2014

812

813 Benn, D.I., Warren, C.W. and Mottram, R.H., (2007), Calving processes and the dynamics of
814 calving glaciers, *Earth-Sci. Rev.*, 82 (3-4), 143-179

815

- 816 Berglund, (2004), Holocene shore displacement and chronology in Ångermanland, eastern
817 Sweden, the Scandinavian glacio-isostatic uplift centre, *Boreas*, 33, 48-60
818
- 819 Berglund, M., (2005), The Holocene shore displacement of Gästrikland, eastern Sweden: a
820 contribution to the knowledge of Scandinavian glacio-isostatic uplift, *J. Quaternary Sci.*, 20
821 (6), 519-531
822
- 823 Björk, S., (1995), A review of the history of the Baltic Sea, 13.0-8.9 ka BP, *Quatern. Int.*, 27,
824 19-40
825
- 826 Boulton, G.S., Dongelmans, P., Punkari, M. and Broadgate, M., (2001) Palaeoglaciology of
827 an ice sheet through a glacial cycle: the European ice sheet through the Weichselian,
828 *Quaternary Sci. Rev.*, 20, 591-625.
829
- 830 Carlson, A.E., (2013), The Younger Dryas Climate Event, in: Elias, S.A. (ed.), *The*
831 *Encyclopedia of Quaternary Science*, vol. 3, 126-134, Elsevier, Amsterdam
832
- 833 Carlson, A.E., Anslow, F.S., Obbink, E.A., LeGrande, A.N., Ullman, D.J. and Licciardi, J.M.,
834 (2009), Surface-melt driven Laurentide Ice Sheet retreat during the early Holocene, *Geophys.*
835 *Res. Lett.*, 36, L24502, doi: 10.1029/2009GL040948.
836
- 837 Carr, J.R., Vieli, A., Stokes, C.R., Jamieson, S.S.R., Palmer, S.J., Cristoffersen, P.,
838 Dowdeswell, J.A., Nick, F.M., Blankenship, D.D. and Young, D.A., (2015), Basal
839 topographic controls on rapid retreat of Humboldt Glacier, northern Greenland, *J. Glaciol.*, 61
840 (225), 137-150
841
- 842 Chauché, N., Hubbard, A., Gascard, J.-C., Box, J.E., Bates, R., Koppes, M., Sole, A.,
843 Christoffersen, P. and Patton, H., (2014), Ice-ocean interaction and calving front morphology
844 at two west Greenland tidewater outlet glaciers, *Cryosphere*, 8, 1457-1468
845
- 846 Clason, C.C., Applegate, P. and Holmlund, P., (2014), Modelling Late Weichselian evolution
847 of the Eurasian ice sheets forced by surface meltwater-enhanced basal sliding, *J. Glaciol.*, 60
848 (219), 29-40
849
- 850 Clason, C.C., Mair, D.W.F., Nienow, P.W., Bartholomew, I.D., Sole, A., Palmer, S. and
851 Schwanghart, W., (2015), Modelling the transfer of supraglacial meltwater to the bed of
852 Leverett Glacier, Southwest Greenland, *Cryosphere*, 9, 123-138
853
- 854 Colgan, W., Rajaram, H., Abdalati, W., McCutchan, C., Mottram, R., Moussavi, M.S. and
855 Grigsby, S., (2016), Glacier crevasses: Observations, models, and mass balance implications,
856 *Rev. Geophys.*, 54, 119-161
857
- 858 Cook, A.J., Vaughan, D.G., Luckman, A.J. and Murray, T., (2014), A new Antarctic
859 Peninsula glacier basin inventory and observed area changes since the 1940s, *Antarct. Sci.*, 26
860 (6), 614-624
861
- 862 Cowton, T., Nienow, P., Sole, A., Wadham, J., Lis, G., Bartholomew, I., Mair, D. and
863 Chandler, D., (2013), Evolution of drainage system morphology at a land-terminating
864 Greenlandic outlet glacier, *J. Geophys. Res.: Earth Surf.*, 118, 1-13,
865 doi:10.1029/2012JF002540

- 866
867 DeConto, R.M. and Pollard, D., (2016), Contribution of Antarctica to past and future sea-level
868 rise, *Nature*, 531, 591-597, doi:10.1038/nature17145
869
870 De Geer, G., (1940), *Geochronologia Suecica Principes*, *Kungliga Svenska*
871 *Vetenskapsakademiens Handlingar III*, 18, 6.
872
873 Doyle, S.H., Hubbard, A., Fitzpatrick, A.A.W., van As, D., Mikkelsen, A.B., Pettersson, R.
874 and Hubbard, B., (2014), Persistent flow acceleration within the interior of the Greenland Ice
875 Sheet, *Geophys. Res. Lett.*, 41, 899-905
876
877 Enderlin, E.M. and Howat, I.M., (2013), Submarine melt rate estimates for floating termini of
878 Greenland outlet glaciers (2000-2010), *J. Glaciol.*, 59 (213), 67-75
879
880 Ettema, J., van den Broeke, M.R., van Meijgaard, E., van de Berg, W.J., Bamber, J.L., Box,
881 J.E. and Bales, C., (2009), Higher surface mass balance of the Greenland ice sheet revealed by
882 high-resolution climate modeling, *Geophys. Res. Lett.*, 36, L12501,
883 doi:10.1029/2009GL038110
884
885 Fowler, A.C., (2010), Weertman, Lliboutry and the development of sliding theory, *J. Glaciol.*,
886 56 (200), 965-972
887
888 Forsström, P., Sallasmaa, O., Greve, R. and Zwinger, T., (2003), Simulation of fast-flow
889 features of the Fennoscandian ice sheet during the Last Glacial Maximum, *Ann. Glaciol.*, 37,
890 383-389
891
892 Glen, J.W., (1955), The creep of polycrystalline ice, *P. Roy. Soc. Lond. A Mat.*, 228 (1175),
893 519-538
894
895 Greenwood, S.L., Clason, C.C., Mikko, H., Nyberg, J., Peterson, G. and Smith, C.A., (2015),
896 Integrated use of LiDAR and multibeam bathymetry reveals onset of ice streaming in the
897 northern Bothnian Sea, *GFF*, 137, 284-292, DOI:10.1080/11035897.2015.1055513
898
899 Greenwood, S.L., Clason, C.C., Nyberg, J., Jakobsson, M. and Holmlund, P., (in press), The
900 Bothnian Sea ice stream: early Holocene retreat dynamics of the south-central Fennoscandian
901 Ice Sheet, *Boreas*, DOI 10.1111/bor.12217
902
903 Gudmundsson, G.H., Krug, J., Durand, G., Favier, L. and Gagliardini, O., (2012), The
904 stability of grounding lines on retrograde slopes, *Cryosphere*, 6, 1497-1505
905
906 Hedenström, A. and Risberg, J., (1999), Early Holocene shore-displacement in southern
907 central Sweden as recorded in elevated isolated basins, *Boreas*, 28, 490-504
908
909 Hochstein, M.P., Watson, M.I., Melengreau, B., Nobes, D.C. and Owens, I., (1998), Rapid
910 melting of the terminal section of the Hooker Glacier (Mt Cook National Park, New Zealand,
911 *New Zeal. J. Geol. Geop.*, 41 (3), 203-218
912
913 Holmlund, P. and Fastook, J., (1993), Numerical modelling provides evidence of a Baltic Ice
914 Stream during the Younger Dryas, *Boreas*, 22 (2), 77-86
915

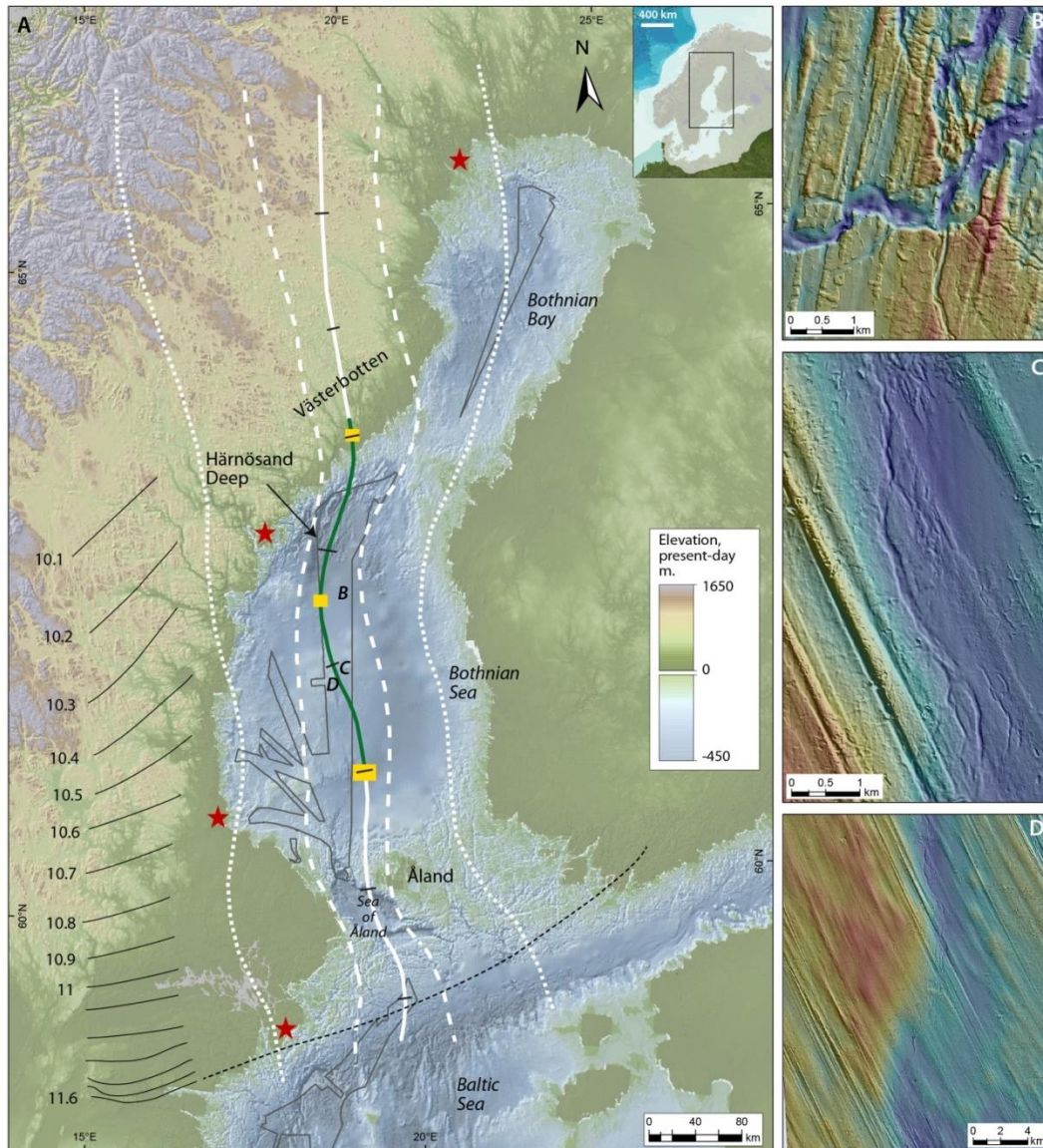
- 916 Hughes, A.L.C., Gyllencreutz, R., Lohne, Ø.S., Mangerud, J. and Svendsen, J.I., (2016), The
917 last Eurasian ice sheets – a chronological database and time-slice reconstruction, DATED-1,
918 *Boreas*, 45, 1-45, 10.1111/bor.12142. ISSN 0300-9483
919
- 920 Jacobs, S.S., Jenkins, A., Giulivi, C.F. and Dutrieux, P., (2011), Stronger ocean circulation
921 and increased melting under Pine Island Glacier ice shelf, *Nature Geoscience*, 4, 519-523,
922 doi:10.1038/ngeo1188
923
- 924 Jakobsson, M., Anderson, J.B., Nitsche, F.O., Dowdeswell, J.A., Gyllencreutz, R., Kirchner,
925 N., O'Regan, M.A., Alley, R.B., Anandakrishnan, S., Mohammad, R., Eriksson, B.,
926 Fernandez, R., Kirchner, A., Minzoni, R., Stollendorf, T., and Majewski, W., (2011), Geological
927 record of ice shelf breakup and grounding line retreat, Pine Island Bay, West Antarctica,
928 *Geology*, 39, (7), 691-694
929
- 930 Jamieson, S.S.R., Vieli, A., Livingstone, S.J., Ó Cofaigh, C., Stokes, C., Hillenbrand, C.-D.
931 and Dowdeswell, J.A., (2012), Ice-stream stability on a reverse bed slope, *Nature Geoscience*,
932 5, 799-802
933
- 934 Jamieson, S.S.R., Vieli, A., Ó Cofaigh, C., Stokes, C.R., Livingstone, S.J. and Hillenbrand,
935 C.-D., (2014), Understanding controls on rapid ice-stream retreat during the last deglaciation
936 of Marguerite Bay, Antarctica, using a numerical model, *J. Geophys. Res.: Earth Surf.*, 119,
937 1-17, doi:10.1002/2013JF002934
938
- 939 Jenkins, A., (2011), Convection-driven melting near the grounding lines of ice shelves and
940 tidewater glaciers, *J. Phys. Oceanogr.*, 41, 2279-2294, doi: 10.1175/JPO-D-11-03.1
941
- 942 Johansson, P., Lunkka, J.P. and Sarala, P., (2011), The Glaciation of Finland, in: Ehlers, J.,
943 Gibbard, P.L. and Hughes, P.D., (ed.), Quaternary Glaciations – Extent and Chronology, A
944 closer look, *Dev. Quatern. Sci.*, 15, 105-116, Elsevier, Amsterdam.
945
- 946 Jones, R.S., Mackintosh, A.N., Norton, K.P., Golledge, N.R., Fogwill, C.J., Kubik, P.W.,
947 Christl, M. and Greenwood, S.L., (2015), Rapid Holocene thinning of an East Antarctic outlet
948 glacier driven by marine ice sheet instability, *Nature Communications*, 6, 8910,
949 doi:10.1038/ncomms9910
950
- 951 Joughin, I., Smith, B.E. and Abdalati, W., (2010), Glaciological advances made with
952 interferometric synthetic aperture radar, *J. Glaciol.*, 56 (200), 1026-1042
953
- 954 Joughin, I. and Alley, R.B., (2011), Stability of the West Antarctic ice sheet in a warming
955 world, *Nature Geoscience*, 4 (8), 506-513
956
- 957 Kjeldsen, K.K., Korsgaard, N.J., Bjørk, A.A., Khan, S.A., Box, J.E., Funder, S., Larsen, N.K.,
958 Bamber, J.L., Colgan, W., van den Broeke, M., Siggaard-Andersen, M.-L., Nuth, C.,
959 Schomacker, A., Andresen, C.S., Willerslev, E. and Kjær, K.H., (2015), Spatial and temporal
960 distribution of mass loss from the Greenland Ice Sheet since AD 1900, *Nature*, 528, 396-400
961
- 962 Kleman, J., Hättestrand, C., Borgström, I. and Stroeven, A., (1997), Fennoscandian
963 palaeoglaciology reconstructed using a glacial geological inversion model, *J. Glaciol.*, 43,
964 283-299.
965

- 966 Lantmäteriet, (2015), Produktbeskrivning: GSD-Höjddata, grid 50+, Lantmäteriet, Gävle
967
- 968 Lea, J.M., Mair, D.W.F., Nick, F.M., Rea, B.R., van As, D., Morlighem, M., Nienow, P.W.
969 and Weidick, A., (2014a), Fluctuations of a Greenlandic tidewater glacier driven by changes
970 in atmospheric forcing: observations and modelling of Kangiata Nunaata Sermia, 1859-
971 present, *Cryosphere*, 8, 2031-2045
972
- 973 Lea, J.M., Mair, D.W.F., Nick, F.M., Rea, B.R., Weidick, A., Kjær, K.H., Morlighem, M.,
974 van As, D. and Schofield, J.E., (2014b), Terminus-driven retreat of a major southwest
975 Greenland tidewater glacier during the early 19th century: insights from glacier reconstructions
976 and numerical modelling, *J. Glaciol.*, 60 (220), 333-344
977
- 978 Lindén, M., Möller, P., Björck, S. and Sandgren, P., (2006), Holocene shore displacement and
979 deglaciation chronology in Norrbotten, Sweden, *Boreas*, 35, 1-22
980
- 981 Livingstone, S.J., Ó Cofaigh, C., Stokes, C.R., Hillenbrand, C.-D., Vieli, A. and Jamieson, S.S.R.,
982 (2012), Antarctic palaeo-ice streams, *Earth-Sci. Rev.*, 111, 90-128
983
- 984 Luckman, A., Benn, D.I., Cottier, F., Bevan, S., Nilsen, F. and Inall, M., (2015), Calving rates at
985 tidewater glaciers vary strongly with ocean temperature, *Nat. Commun.*, 6:8566, doi:
986 10.1038/ncomms9566
987
- 988 Lundqvist, J., (2007), Surging ice and break-down of an ice dome – a deglaciation model for
989 the Gulf of Bothnia, *GFF*, 129, 329-336.
990
- 991 Meyaud, J.R., Banwell, A.F., Arnold, N.S. and Willis, I.C., (2014), Modeling the response of
992 subglacial drainage at Paakitsoq, west Greenland, to 21st century climate change, *J. Geophys.*
993 *Res.: Earth Surf.*, 119 (12), 2619-2634
994
- 995 Motyka, R.J., Hunter, L., Echelmeyer, K.A. and Connor, C., (2003), Submarine melting at the
996 terminus of a temperate tidewater glacier, LeConte Glacier, Alaska, U.S.A., *Ann. Glaciol.*, 36,
997 57-65
998
- 999 Murray, T., Scharer, K., James, T.D., Dye, S.R., Hanna, E., Booth, A.D., Selmes, N.,
1000 Luckman, A., Hughes, A.L.C., Cook, S. and Huybrechts, P., (2010), Ocean regulation
1001 hypothesis for glacier dynamics in southeast Greenland and implications for ice sheet mass
1002 changes, *J. Geophys. Res.*, 115, F03026, doi:10.1029/2009JF001522
1003
- 1004 Murray, T., Scharer, K., Selmes, N., Booth, A.D., James, T.D., Bevan, S.L., Bradley, J.,
1005 Cook, S., Cordero Llana, L., Drocourt, Y., Dyke, L., Goldsack, A., Hughes, A.L., Luckman,
1006 A.J. and McGovern, J., (2015), Extensive retreat of Greenland tidewater glacier, 2000-2010,
1007 *Arc. Antarc. Alp. Res.*, 47 (3), 427-447
1008
- 1009 Muschitiello, F., Pausata, F.S.R., Watson, J.E., Smittenberg, R.H., Salih, A.A.M., Brooks,
1010 S.J., Whitehouse, N.J., Karlatou-Charalampopoulou, A. and Wohlfarth, B., (2015),
1011 Fennoscandian freshwater control on Greenland hydroclimate shifts at the onset of the
1012 Younger Dryas, *Nature Communications*, 6, 8939
1013
- 1014 Nick, F.M., Vieli, A., Howat, I.M. and Joughin, I., (2009), Large-scale changes in Greenland
1015 outlet glacier dynamics triggered at the terminus, *Nature Geoscience*, 2, 110-114
1016

- 1017 Nick, F.M., van der Veen, C.J., Vieli, A. and Benn, D.I., (2010), A physically based calving
1018 model applied to marine outlet glaciers and implications for the glacier dynamics, *J. Glaciol.*,
1019 56 (199), 781-794
1020
- 1021 Nick, F.M., Luckman, A., Vieli, A., van der Veen, C.J., van As, D., van de Wal, R.S.W.,
1022 Pattyn, F., Hubbard, A.L. and Floricioiu, D., (2012), The response of Petermann Glacier,
1023 Greenland, to large calving events, and its future stability in the context of atmospheric and
1024 oceanic warming, *J. Glaciol.*, 58 (208), 229-239
1025
- 1026 Nye, J.F., (1957), The distribution of stress and velocity in glaciers and ice-sheets, *P. Roy.*
1027 *Soc. Lond. A. Mat.*, 239 (1216), 113-133
1028
- 1029 Pollard, D., DeConto, R.M. and Alley, R.B., (2015), Potential Antarctic Ice Sheet retreat
1030 driven by hydrofracturing and ice cliff failure, *Earth Planet. Sci. Lett.*, 412, 112-121
1031
- 1032 Punkari, M., (1980), The ice lobes of the Scandinavian ice sheet during the deglaciation of
1033 Finland, *Boreas*, 9, 307-310.
1034
- 1035 Rea, B.R. and Evans, D.J.A., (2007), Quantifying climate and glacier mass balance in north
1036 Norway during the Younger Dryas, *Palaeogeog. Palaeoclim.*, 246, 307-330
1037
- 1038 Reimer, P.J., Bard, E., Bayliss, A., Beck, J.W., Blackwell, P.G., Bronk Ramsey, C., Buck,
1039 C.E., Cheng, H., Edwards, R.L., Friedrich, M., Grootes, P.M., Guilderson, T.P., Haflidason,
1040 H., Hajdas, I., Hatte, C., Heaton, T.J., Hoffman, D.L., Hogg, A.G., Hughen, K.A., Felix
1041 Kaiser, K., Kromer, B., Manning, S.W., Niu, M., Reimer, R.W., Richards, D.A., Scott, E.M.,
1042 Southon, J.R., Staff, R.A., Turney, C.S.M. and van der Plicht, J., (2013), IntCal13 and
1043 Marine13 radiocarbon age calibration curves 0-50,000 years cal BP, *Radiocarbon*, 55 (4),
1044 1869-1887
1045
- 1046 Rignot, E., Koppes, M. and Velicogna, I., (2010), Rapid submarine melting of the calving
1047 faces of West Greenland glaciers, *Nature Geoscience*, 3, 187-191
1048
- 1049 Rignot, E., Jacobs, S., Mouginot, J. and Scheuchl, B., (2013), Ice-shelf melting around
1050 Antarctica, *Science*, 341, 266-270, DOI: 10.1126/science.1235798
1051
- 1052 Rippin, D.M., Vaughan, D.G. and Corr, H.F.J., (2011), The basal roughness of Pine Island
1053 Glacier, West Antarctica, *J. Glaciol.*, 57 (201), 67-76
1054
- 1055 Schoof, C., (2007), Ice sheet grounding line dynamics: Steady states, stability, and hysteresis,
1056 *J. Geophys. Res.*, 112, F03S28
1057
- 1058 Siegert, M.J. and Dowdeswell, J.A., (2004), Numerical reconstructions of the Eurasian Ice
1059 Sheet and climate during the Late Weichselian, *Quaternary Sci. Rev.*, 23, 1273-1283
1060
- 1061 Sole, A., Nienow, P., Bartholomew, I., Mair, D., Cowton, T., Tedstones, A. and King, M.A.,
1062 (2013), Winter motion mediates dynamic response of the Greenland Ice Sheet to warmer
1063 summers, *Geophys. Res. Lett.*, 40, 3940-3944
1064
1065

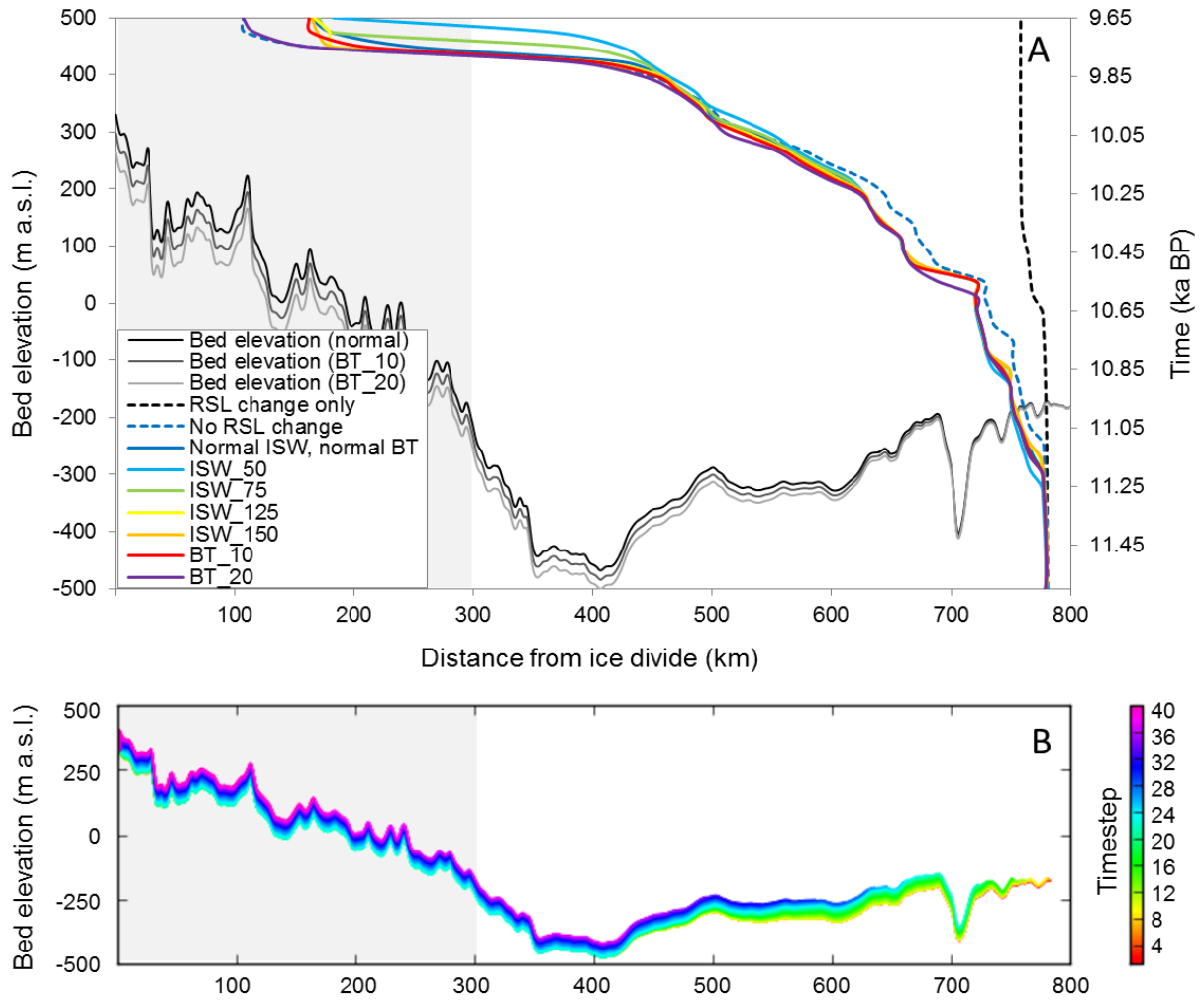
- 1066 Straneo, F., Heimbach, P., Sergienko, O., Hamilton, G., Catania, G., Griffies, S., Hallberg, R.,
1067 Jenkins, A., Joughin, I., Motyka, R., Pfeffer, T.W., Price, S.F., Rignot, E., Scambos, T.,
1068 Truffer, M. and Vieli, A., (2013), Challenges to understanding the dynamic response of
1069 Greenland's marine terminating glaciers to oceanic and atmospheric forcing, *B. Am. Meteorol.*
1070 *Soc.*, 94 (8), 1131-1144
1071
- 1072 Stroeven, A.P., Hättestrand, C., Kleman, J., Heyman, J., Fabel, D., Fredin, O., Goodfellow,
1073 B.W., Harbor, J.M., Jansen, J.D., Olsen, L., Caffee, M.W., Fink, D., Lundqvist, J., Rosqvist,
1074 G.C., Strömberg, B. and Jansson, K.N., (2016), Deglaciation of Fennoscandia, *Quaternary*
1075 *Sci. Rev.*, 147, 91-121.
1076
- 1077 Strömberg, B., (1989), Late Weichselian deglaciation and clay varve chronology in east-
1078 central Sweden, *Sveriges Geologiska Undersökning Ser. Ca*, 73.
1079
- 1080 Sundal, A.V., Shepherd, A., Nienow, P., Hanna, E., Palmer, S. and Huybrechts, P., (2011),
1081 Melt-induced speed-up of Greenland ice sheet offset by efficient subglacial drainage, *Nature*,
1082 469(7331), 521-4
1083
- 1084 Thomas, R.H., (2007), Tide-induced perturbations of glacier velocities, *Global Planet.*
1085 *Change*, 59 (1-4), 217-224
1086
- 1087 Van de Wal, R.S.W., Smeets, C.J.P.P., Boot, W., Stoffelen, M., van Kampen, R., Doyle, S.H.,
1088 Wilhelms, F., van den Broeke, M.R., Reijmer, C.H., Oerlemans, J. and Hubbard, A., (2015),
1089 Self-regulation of ice flow varies across the ablation area in south-west Greenland,
1090 *Cryosphere*, 9, 603-611
1091
- 1092 Van den Broeke, M., Bamber, J., Ettema, J., Rignot, E., Schrama, E., van de Berg, W.J., van
1093 Meijgaard, E., Velicogna, I. and Wouters, B., (2009), Partitioning recent Greenland mass loss,
1094 *Science*, 326, 984-986
1095
- 1096 Van der Veen, C.J. and Whillans, I.M., (1996), Model experiments on the evolution and
1097 stability of ice streams, *Ann. Glaciol.*, 23, 129-137
1098
- 1099 Van der Veen, C.J., (1999), *Fundamentals of glacier dynamics*, Rotterdam, A.A. Balkema
1100
- 1101 Vieli, A. and Payne, A.J., (2005), Assessing the ability of numerical ice sheet models to
1102 simulate grounding line migration, *J. Geophys. Res.*, 110 (F1), F01003,
1103 10.1029/2004JF000202
1104
- 1105 viewfinderpanoramas.org, (2014), 1 arc second digital elevation data for Northern Europe,
1106 accessed July 2015
1107
- 1108 Weertman, J., (1974), Stability of the junction of an ice sheet and an ice shelf, *J. Glaciol.*, 13,
1109 3-11
1110
- 1111 Whillans, I.M. and van der Veen, C.J., (1997), The role of lateral drag in the dynamics of Ice
1112 Stream B, Antarctica, *J. Glaciol.*, 43 (144), 231-237
1113
1114

- 1115 Winsborrow, M.C.M., Andreassen, K., Corner, G.D. and Laberg, J.S., (2010), Deglaciation of
1116 a marine-based ice sheet: Late Weichselian palaeo-ice dynamics and retreat in the southern
1117 Barents Sea reconstructed from onshore and offshore glacial geomorphology, *Quaternary Sci.*
1118 *Rev.*, 29, 424-442
1119
- 1120 Zwally, H.J., Abdalati, W., Herring, T., Larson, K., Saba, J. and Steffen, K., (2002), Surface
1121 melt-induced acceleration of Greenland ice-sheet flow, *Science*, 297 (5579), 218-222
1122

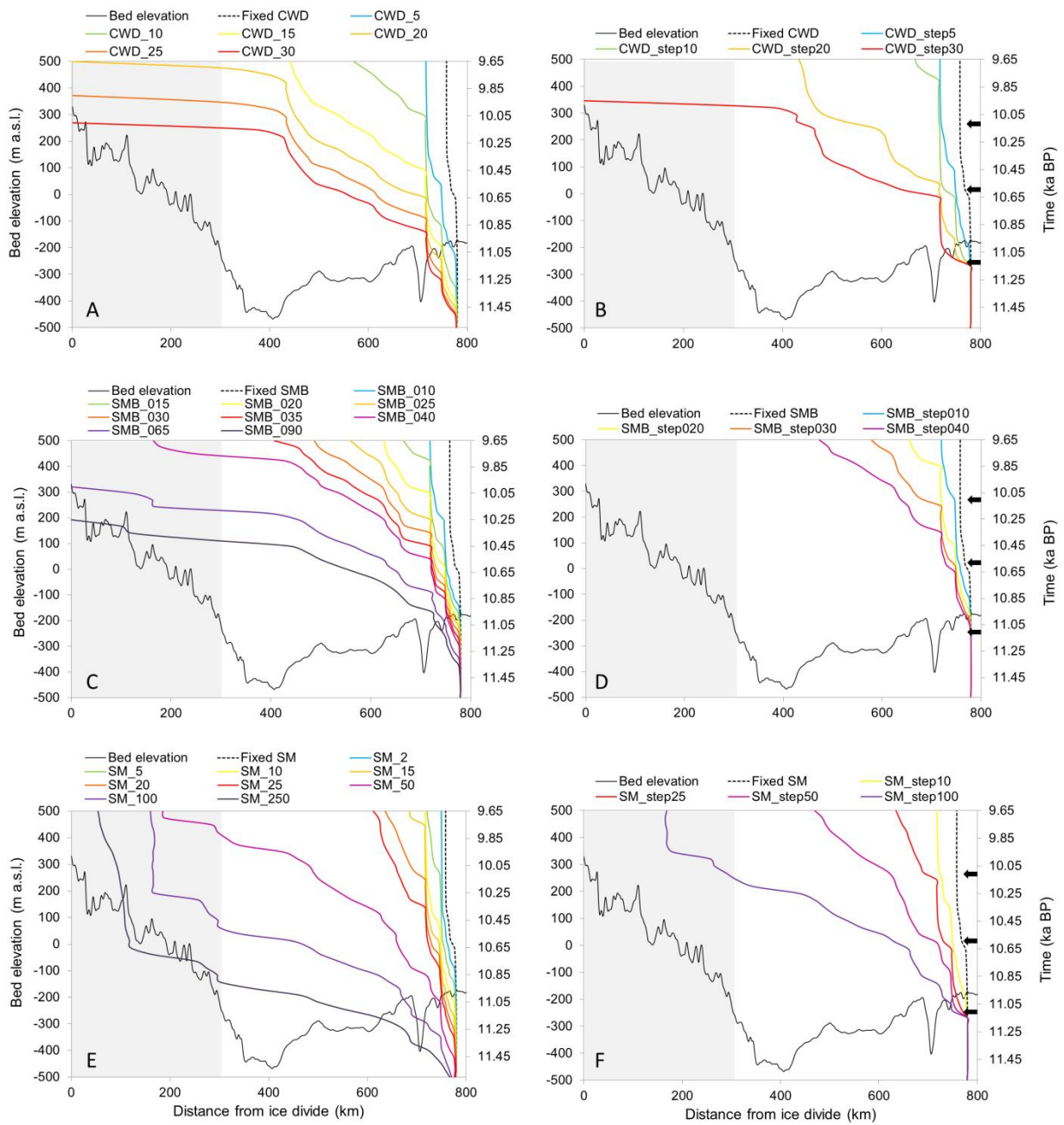


1123
1124

1125 Figure 1. A: Bothnian Sea ice flowline, based on geomorphological interpretations and
1126 estimated maximum and minimum ice stream widths (solid, dashed and dotted white lines
1127 respectively). Black tickmarks at 100 km intervals are placed along the flowline; the green
1128 portion of the line denotes the segment for which there is geomorphological evidence for ice
1129 streaming velocities; yellow rectangles mark identified sticky zones; red stars mark sites of
1130 shoreline displacement data from (north to south) Norrbotten, Ångermanland (Swedish High
1131 Coast), Gästrikland and Södertörn. Areas for which multibeam bathymetry data were
1132 available are outlined in grey. The displayed background bathymetry is from the Baltic Sea
1133 Bathymetry Database (Baltic Sea Hydrographic Commission, 2013); topographic compilation
1134 from viewfinderpanoramas.org (2014). The varve-based deglacial chronology from Stroeven
1135 et al. (2016) between 11.6 and 10.1 ka BP is depicted in black on the left, with the
1136 hypothesised Younger Dryas (11.6 ka BP) limit extended across the Baltic Sea. Inset shows
1137 the Baltic-Bothnian Basins in the context of the Fennoscandian Ice Sheet (including the 21 ka
1138 BP areal ice extent, after Hughes et al., 2016). B-D: extracts from the multibeam data
1139 illustrating mega-scale glacial lineations, indicative of the ice stream pathway flowing SSW in
1140 the upper part of the flowline (B), and SSE downstream (C, D). Large and well-connected
1141 meltwater channel systems overprint and incise the ice stream assemblage (B, C).

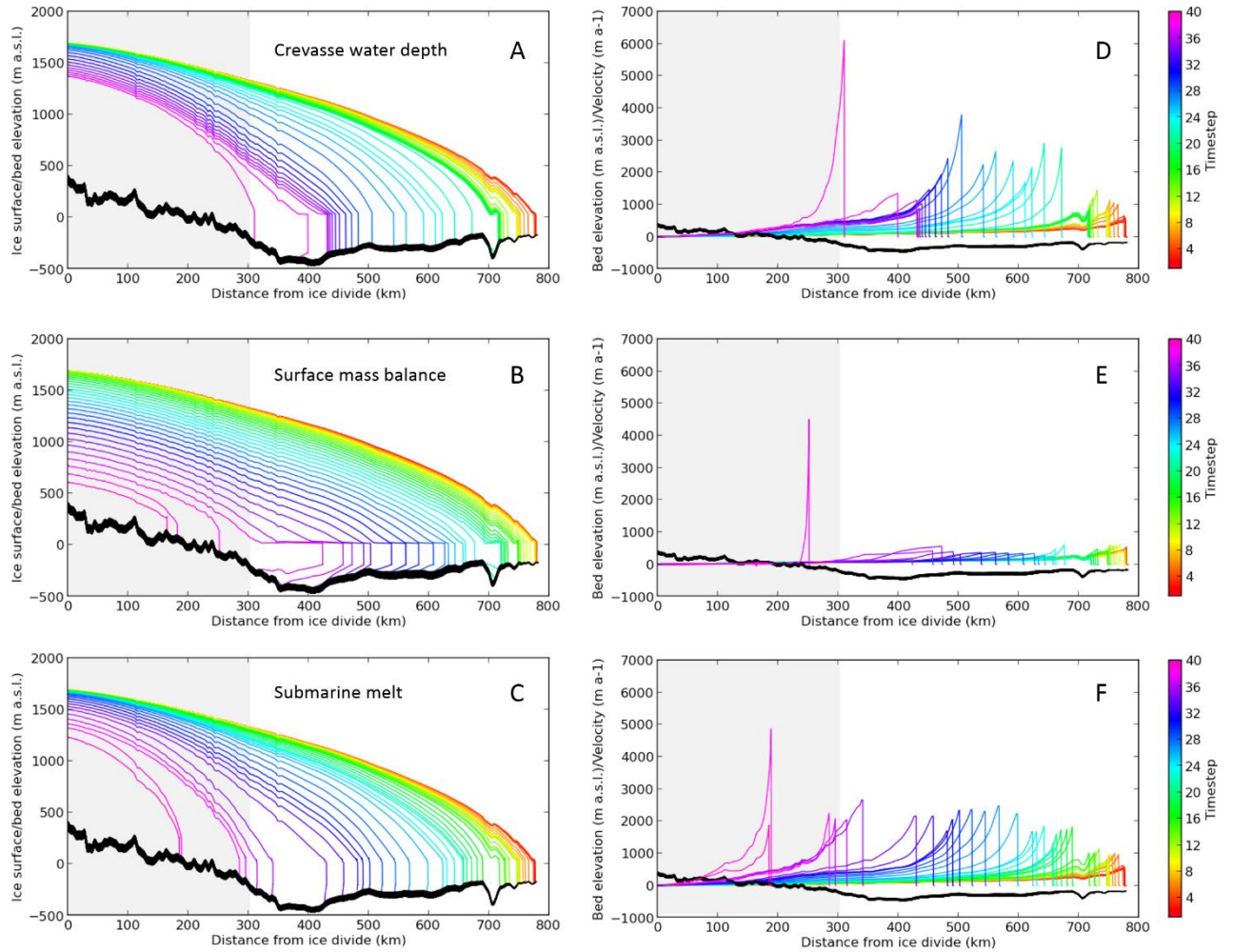


1142
 1143 Figure 2. A: Grounding line retreat for experiments testing sensitivity to the inclusion and
 1144 exclusion of RSL change, changes to ice stream width (ISW) and changes to bed tilt (BT).
 1145 The late Younger Dryas grounding line position is shown to be insensitive to RSL change
 1146 alone (black dashed line). Retreat for ISW and BT tests is forced by surface mass balance
 1147 scenario SMB_040, and the dashed blue line represents running SMB_40 with no RSL
 1148 change. B: Changes to bed elevation along with flowline over a 2000 year model run (one
 1149 profile produced every 50 years for 40 timesteps), forced by RSL change. The grey area
 1150 represents the less well-constrained upper portion of the flowline, above present-day sea level,
 1151 here and in subsequent figures.
 1152



115
1154
1155
1156
1157
1158
1159
1160
1161
1162
1163
1164
1165

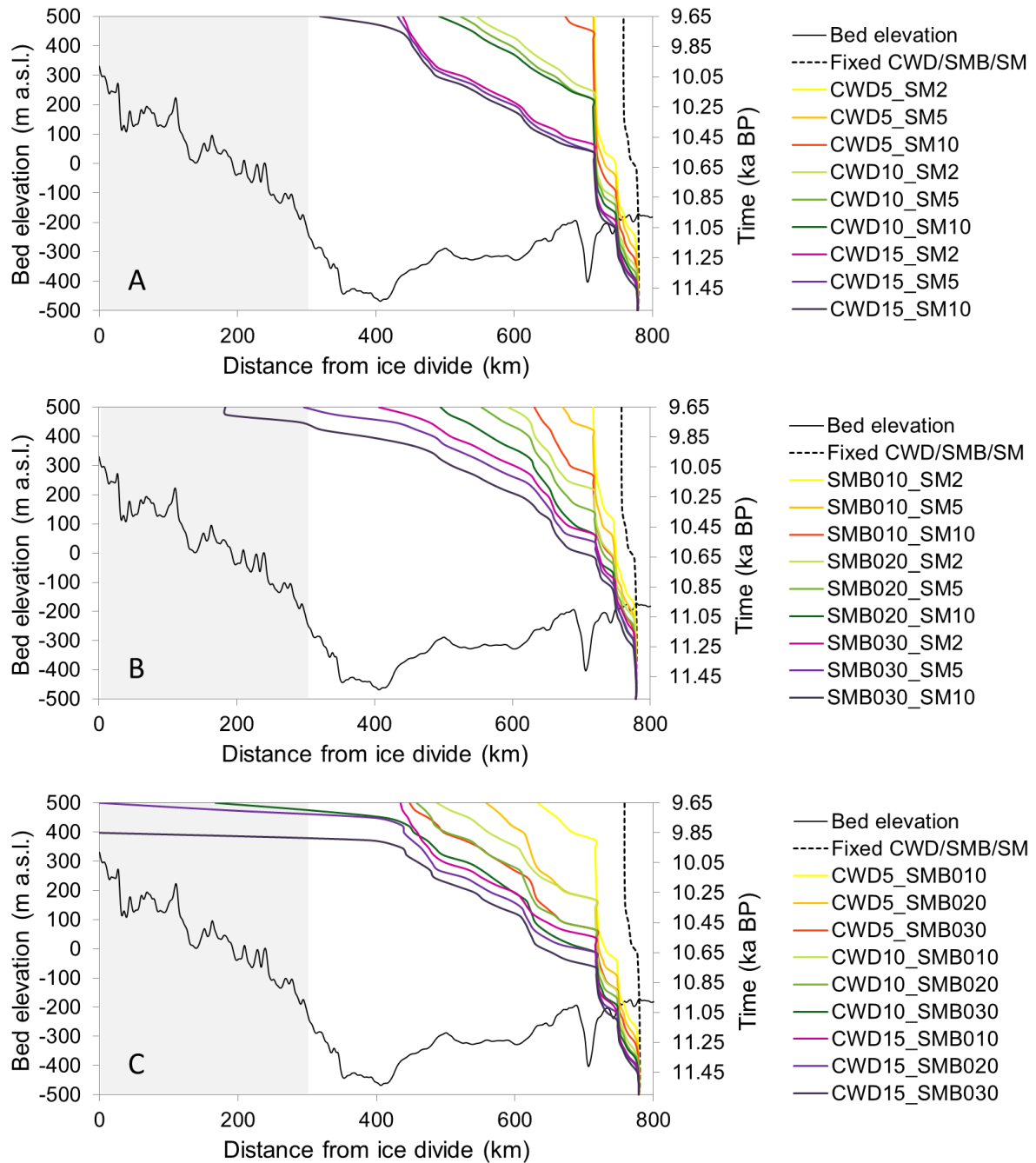
Figure 3. Grounding line retreat sensitivity to crevasse water depth (CWD), surface mass balance (SMB) and submarine melting (SM), for linear (A, C and E) and step-wise (B, D and F) forcing experiments. Black arrows indicate the timing of step changes in forcing.



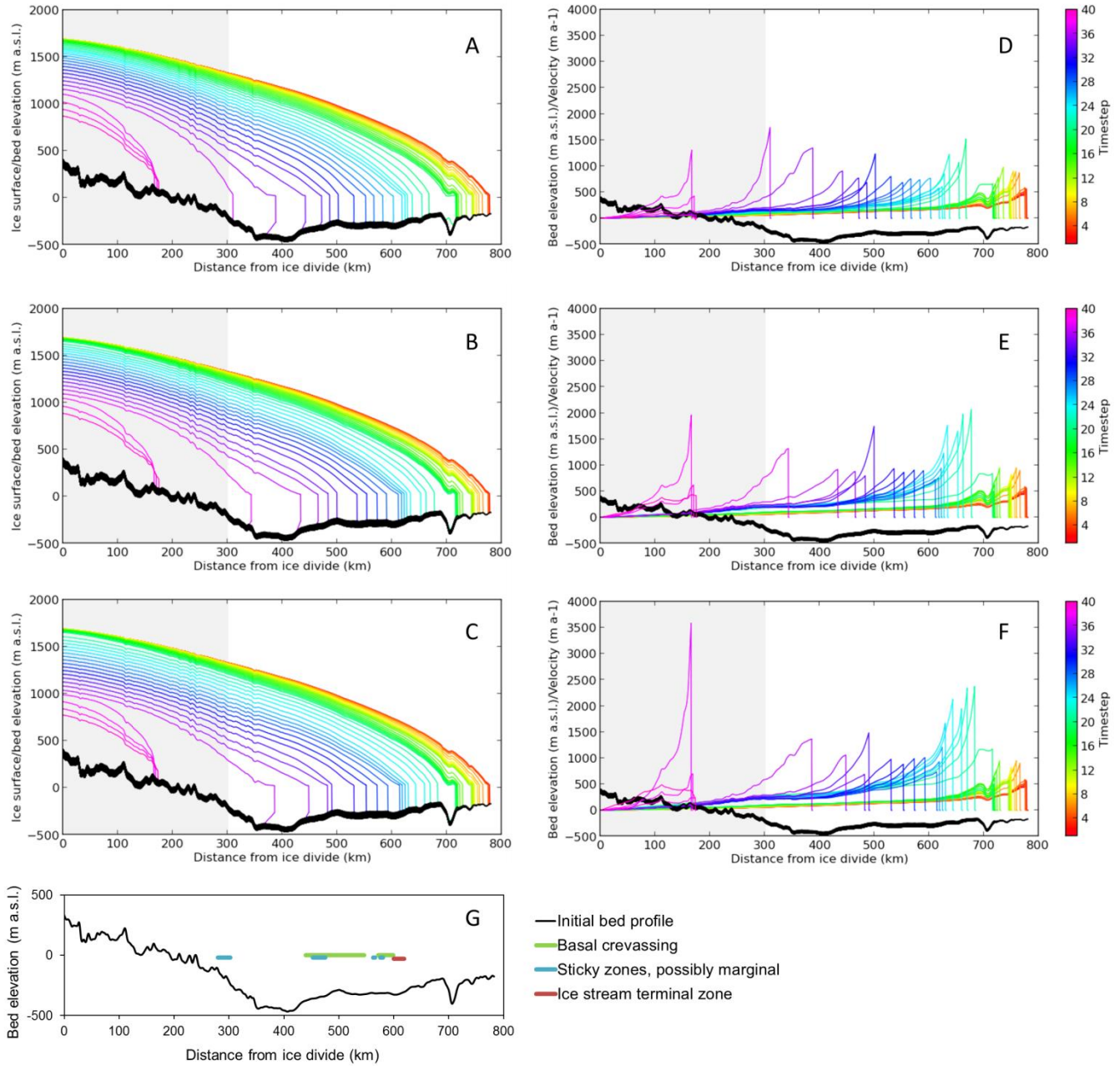
1166

1167 Figure 4. Comparison of terminus retreat and ice surface evolution for experiments: CWD_20
 1168 (A), SMB_040 (B), and SM_50 (C), plotted for each 50-year timestep over a total of 40
 1169 timesteps (2000 years). The thickness of the bed (black line) depicts total RSL change over
 1170 the model run. D, E and F illustrate ice surface velocities along the flowline at each 50 year
 1171 timestep for experiments CWD_20, SMB_040, and SM_50 respectively. Note the experiment
 1172 CWD_20 retreats fully to the ice divide within the final 50 year timestep.

1173

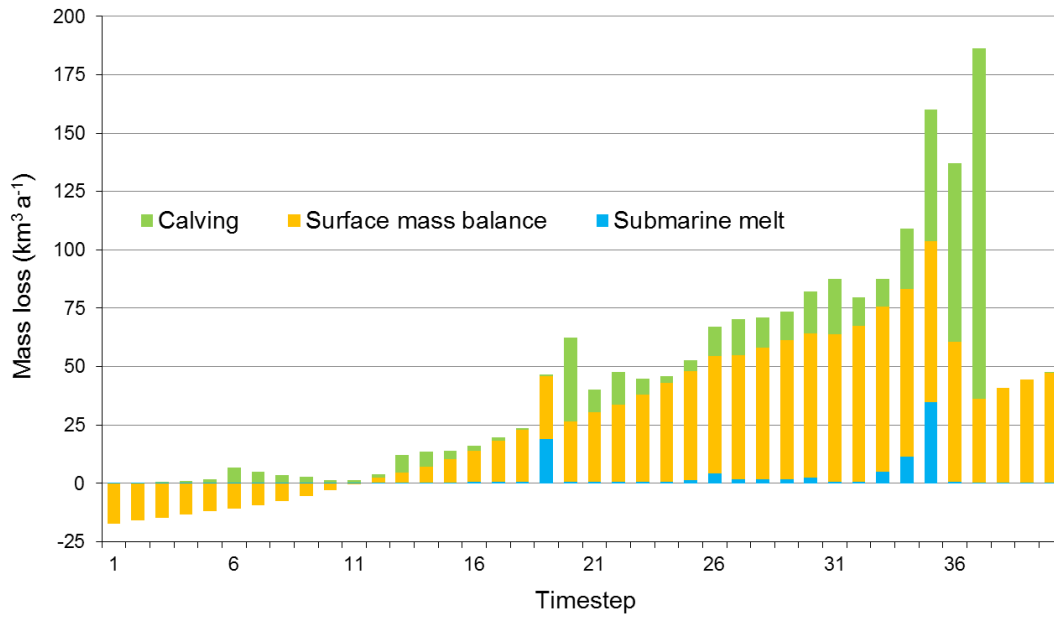


1174
 1175 Figure 5. Grounding line retreat for combined linear forcing experiments, testing sensitivity to
 1176 A) crevasse water depth (CWD) and submarine melting (SM), B) surface mass balance
 1177 (SMB) and submarine melting (SM), and C) crevasse water depth (CWD) and surface mass
 1178 balance (SMB).
 1179



1180
 1181
 1182 Figure 6. Comparison of terminus retreat and ice surface evolution for enhanced basal sliding
 1183 experiments: CWD10_SMB030_SM5_BF1 (A), CWD10_SMB030_SM5_BF08 (B), and
 1184 CWD10_SMB030_SM5_BF07 (C), plotted for each 50-year timestep over a total of 40
 1185 timesteps (2000 years). D, E and F illustrate ice surface velocities along the flowline at each
 1186 50 year timestep for experiments CWD10_SMB030_SM5_BF1,
 1187 CWD10_SMB030_SM5_BF08, and CWD10_SMB030_SM5_BF07 respectively. G depicts
 1188 the locations of ice stream termination, sticky zones, and basal crevassing, as inferred from
 1189 geomorphological analysis of multibeam data.

1190
 1191
 1192



1193

1194 Figure 7. Rate of mass loss at each 50 year model timestep for experiment
1195 CWD10_SMB030_SM5_BF1, partitioned by calving, surface mass balance, and submarine
1196 melt. Note that calving is a by-product of crevasse water depth, but that calving events are not
1197 solely attributable to crevasse water depth.

1198

1199

1200

1201

1202

1203

1204

1205

1206

1207

1208

1209

1210

1211

Description	Value
Acceleration due to gravity, g	9.8 m s ⁻²
Density of ice, ρ_i	917 kg m ⁻³
Density of proglacial water, ρ_p	1000 kg m ⁻³
Density of meltwater, ρ_w	1000 kg m ⁻³
Glen's flow law exponent, n	3
Glen's flow law coefficient, A	2.9 x 10 ⁻¹⁷ Pa ⁻³ a ⁻¹ (ice temperature -5°C)
Friction exponent, m	3
Basal friction parameter, μ	1 (unless otherwise stated)
Grid size (variable)	c. 500 m
Model timestep	0.005 years

1212
1213
1214
1215
1216
1217
1218
1219
1220
1221
1222
1223
1224
1225
1226
1227
1228
1229
1230
1231
1232
1233
1234
1235
1236
1237
1238
1239
1240
1241
1242
1243
1244
1245
1246
1247
1248

Table 1. Values for physical parameters and constants applied in the model.

Experiment set	System geometry		Crevasse water depth (m)		Mass balance at sea level ($\text{m a}^{-1} \text{m}^{-2}$)		Submarine melt (m a^{-1})	
	<i>Bed profile</i>	<i>Ice stream width</i>	<i>Linear increase over 500 years from 95</i>	<i>Step increase every 500 years from 95</i>	<i>Linear decrease over 500 years from -0.5</i>	<i>Step decrease every 500 years from -0.5</i>	<i>Linear increase over 500 years from 0</i>	<i>Step increase every 500 years from 0</i>
1. Sensitivity to bed topography, ice stream width and RSL change	Normal, 10% tilt, 20% tilt	Average, 50%, 75%, 125%, 150%	Fixed at 95	-	0.4	-	Fixed at 0	-
2. Sensitivity to individual atmospheric forcings	Normal	Average	5, 10, 15, 20, 25, 30	5, 10, 20, 30	0.1, 0.15, 0.2, 0.25, 0.3, 0.35, 0.4, 0.65, 0.9	0.1, 0.2, 0.3, 0.4	Fixed at 0	-
3. Sensitivity to individual marine forcings	Normal	Average	Fixed at 95	-	Fixed at -0.5	-	2, 5, 10, 15, 20, 25, 50, 100, 250	10, 25, 50, 100
4. Sensitivity to combined forcings	Normal	Average	5, 10, 15	-	0.1, 0.2, 0.3	-	2, 5, 10	-

Table 2. Description of experiment sets testing sensitivity to changes in system geometry, and sensitivity to linear and step-wise changes in atmospheric and marine forcings. Experiments with linear changes split the specified forcing value evenly every year per 500 years, and step changes add/subtract the specified value every 500 years (three step changes per 2 kyr run). Each run is 2000 years long.